AMERICAN SOCIETY FOR MICROBIOLOGY | mBio®

RESEARCH ARTICLE

Spindle Dynamics during Meiotic Development of the Fungus *Podospora anserina* Requires the Endoplasmic Reticulum-Shaping Protein RTN1

Antonio de Jesús López-Fuentes,[a] Karime Naid Nachón-Garduño,[a] Fernando Suaste-Olmos,[a] Ariadna Mendieta-Romero,[a] Leonardo Peraza-Reyes[a]

[a]Departamento de Bioquímica y Biología Estructural, Instituto de Fisiología Celular, Universidad Nacional Autónoma de México, Mexico City, Mexico

ABSTRACT The endoplasmic reticulum (ER) is an elaborate organelle composed of distinct structural and functional domains. ER structure and dynamics involve membrane-shaping proteins of the reticulon and Yop1/DP1 families, which promote membrane curvature and regulate ER shaping and remodeling. Here, we analyzed the function of the reticulon (RTN1) and Yop1 proteins (YOP1 and YOP2) of the model fungus *Podospora anserina* and their contribution to sexual development. We found that RTN1 and YOP2 localize to the peripheral ER and are enriched in the dynamic apical ER domains of the polarized growing hyphal region. We discovered that the formation of these domains is diminished in the absence of RTN1 or YOP2 and abolished in the absence of YOP1 and that hyphal growth is moderately reduced when *YOP1* is deleted in combination with *RTN1* and/or *YOP2*. In addition, we found that RTN1 associates with the Spitzenkörper. Moreover, RTN1 localization is regulated during meiotic development, where it accumulates at the apex of growing asci (meiocytes) during their differentiation and at their middle region during the subsequent meiotic progression. Furthermore, we discovered that loss of RTN1 affects ascospore (meiotic spore) formation, in a process that does not involve YOP1 or YOP2. Finally, we show that the defects in ascospore formation of *rtn1* mutants are associated with defective nuclear segregation and spindle dynamics throughout meiotic development. Our results show that sexual development in *P. anserina* involves a developmental remodeling of the ER that implicates the reticulon RTN1, which is required for meiotic nucleus segregation.

IMPORTANCE Meiosis consists of a reductional cell division, which allows ploidy maintenance during sexual reproduction and which provides the potential for genetic recombination, producing genetic variation. Meiosis constitutes a process of foremost importance for eukaryotic evolution. Proper partitioning of nuclei during this process relies on accurate functioning and positioning of the spindle, the microtubule cytoskeletal apparatus that conducts chromosome segregation. In this research, we show that in the model fungus *Podospora anserina* this process requires a protein involved in structuring the endoplasmic reticulum (ER)—the reticulon RTN1. The ER is a complex organelle composed of distinct structural domains, including different peripheral domains and the nuclear envelope. Our findings suggest that spindle dynamics during meiosis relies on remodeling of the ER membrane, which involves the activity of RTN1. Our research discloses that the proteins implicated in shaping the ER are main contributors to the regulation of nuclear dynamics during the sexual cycle.

KEYWORDS endoplasmic reticulum (ER), meiosis, fungi, organelle dynamics, spindle, reticulon, sexual development, Spitzenkörper, organelle structure

Citation López-Fuentes ADJ, Nachón-Garduño KN, Suaste-Olmos F, Mendieta-Romero A, Peraza-Reyes L. 2021. Spindle dynamics during meiotic development of the fungus *Podospora anserina* requires the endoplasmic reticulum-shaping protein RTN1. mBio 12:e01615-21. https://doi.org/10.1128/mBio.01615-21.

Editor Reinhard Fischer, Karlsruhe Institute of Technology (KIT)

Address correspondence to Leonardo Peraza-Reyes, lperaza@ifc.unam.mx.

Received 2 June 2021
Accepted 30 August 2021
Published 5 October 2021

The endoplasmic reticulum (ER) is a multifaceted organelle that is composed of distinct structural and functional domains. The ER consists of a continuous membrane system composed of two major domains—the nuclear envelope (NE) and the peripheral ER—which enclose a common luminal space. The NE is formed by the outer and inner nuclear membranes, which fuse at the nuclear pores, while the peripheral ER consists of a complex network of tubules and cisternal sheets that extends from the NE throughout the cell (1). The ER constitutes the base of the cell endomembrane system and plays a fundamental role in the synthesis, processing, and transport of proteins and lipids (2). In addition, the ER has a central role in calcium homeostasis and signaling (3) and constitutes a hub that integrates complex signaling networks, which maintain cellular homeostasis and regulate cell fate (4–6). The ER participates in the biogenesis of multiple organelles (7) and establishes physical interactions with most membranous cell compartments, performing critical roles in the regulation of their activity and dynamics (1, 8, 9). Moreover, by conforming the NE, the ER is determinant in the regulation of nuclear assembly, dynamics, and remodeling (10–12).

ER structure and dynamics rely on a number of proteins that shape the organelle membranes, facilitate their homotypic fusion, and mediate their association with the cytoskeleton (1). Central to these processes are two conserved families of proteins—the reticulon and Yop1/DP1/REEP proteins—which form oligomers in the ER membrane that promote high membrane curvature (13, 14). Reticulons contain a conserved domain—the reticulon homology domain (RHD)—that is composed of two bipartite hydrophobic segments that form two hairpin-loops with a "W" topology in the ER membrane. Yop1 proteins possess a similar structural domain. These domains have been proposed to produce a hydrophobic wedge in the lipid bilayer promoting membrane bending (1, 15–17). In addition, these proteins possess a second domain required for membrane bending, which consists of a C-terminal amphipathic helix (18, 19). The reticulon and Yop1 proteins facilitate the formation of the peripheral ER tubules and stabilize the edges of ER sheets (14, 20–22). In addition, they have been proposed to stabilize the sites of fusion between the inner and outer membranes of the NE at the nuclear pores (23), and they participate in ER membrane constriction and fission (24).

The reticulon and Yop1/DP1 proteins have been implicated in diverse cellular roles, including the organization of the secretory pathway (25–27), the insertion of the nuclear pore complexes and spindle pole bodies (SPBs; the fungal nuclear membrane-embedded equivalents of centrosomes) in the NE (23, 28), and the regulation of ER segregation during cell division, which ensures inheritance of functional ER (29). Furthermore, the reticulons participate in the formation of the contact sites that the ER establishes with mitochondria (30, 31), peroxisomes (32), and the plasma membrane (33), as well as in the selective elimination of the ER via autophagy (34–37).

Fungi have provided significant insight into the molecular and cellular mechanisms conducting the developmental processes of sexual reproduction, such as karyogamy and meiosis (38–41). Research in fungi has also disclosed critical roles for the ER in these developmental processes. For example, in the yeast *Saccharomyces cerevisiae* karyogamy has long been known to depend on a number of proteins involved in ER protein import, folding, and quality control (42–45), whereas in filamentous ascomycetes the coordination of karyogamy with the meiotic program depends on a conserved ER SUN-domain protein (46). Nevertheless, there is still much to learn about the regulation of ER dynamics, as well as on the specific roles performed by the proteins that structure this organelle during sexual development. Here, we analyze the contribution of the reticulon and Yop1 proteins during sexual development of the model ascomycete *Podospora anserina* and show that the single reticulon protein of this fungus is required for meiotic nucleus segregation.

RESULTS

The *P. anserina* ER. The *P. anserina* life cycle is shown in Fig. S1 in the supplemental material. In order to study the *P. anserina* ER, we analyzed the localization of an

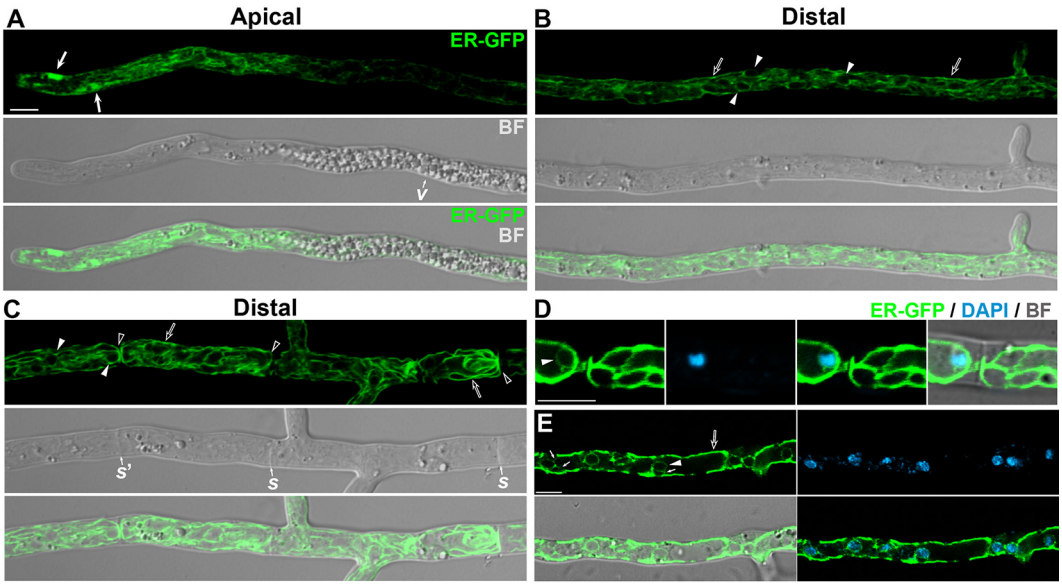

FIG 1 The *Podospora anserina* ER. Confocal microscopy analysis of ER-GFP-labeled ER in different hyphal regions of *P. anserina* young mycelial cultures (≈24 h old). The apical (A) and distal regions of leading hyphae extending approximately 100 μm (B) and 200 μm (C) behind the tip are shown. In panels D and E, the ER is compared to the localization of DAPI-stained nuclei in a leading hypha (D) and in a narrow hypha branching from distal hyphal regions (E). Arrows, apical ER subcompartments; arrowheads, nuclear envelope; open arrows, cortical ER; open arrowheads, cortical ER bordering septa; small arrows in panel E, ER strands connecting the cortical and nuclear ER; *v*, vacuolized hyphal region; *s*, septa; BF, bright field. Bar, 5 μm.

ectopically expressed ER-targeted green fluorescent protein (ER-GFP), which consisted of enhanced GFP (EGFP) flanked by the ER targeting and retention signals of the putative *P. anserina* ER chaperone BiP/Kar2 (47). We have shown that ER-GFP localizes to a large network of interconnected strands extending throughout the hypha (47), with a similar arrangement as that of the ER of other filamentous fungi (48–51). Moreover, we observed that ER-GFP exhibits a polarized distribution in hyphae, including an ER subdomain specifically located in the polarized growing apical region of hyphae (i.e., within the first ≈15 μm extending behind the hyphal tip). This ER subdomain consists of a number of dynamic and pleomorphic ER subcompartments (Fig. 1A), which are interconnected with the peripheral ER strands and which undergo fusion and division events accompanied by directional displacements along hyphae (47).

Additional ER subdomains also display a differential distribution along *P. anserina* hyphae. In growing leading hyphae, the apical ER region was followed by a segment with decreased ER-GFP fluorescence, located in the subapical hyphal region where large vacuoles accumulate (between 42.4 $\pm$ 9 and 84.4 $\pm$ 9 μm behind the hyphal tip, n = 15) (Fig. 1A), suggesting that the ER is partially excluded from this region by its high intracellular crowding. Behind this region, ER-GFP labeled a large network of ER strands throughout hyphae (Fig. 1B), which were more prominent toward the septate hyphal region (i.e., ≈250 μm behind the hyphal tip) (Fig. 1C). The ER-GFP-labeled ER network included a number of strands underlying the cell periphery, likely representing the plasma membrane-associated ER (Fig. 1B and C). In septate hyphal regions, these cortical ER strands also bordered the septa delimiting hyphal compartments (Fig. 1C). As previously described for the *Aspergillus oryzae* ER (49), septa were frequently flanked by parallel ER strands from adjacent compartments (Fig. 1C). However, we also observed continuity of the ER through the septal pores communicating between cell compartments (Movie S1). Consistent with localization to the NE, we found that ER-GFP also labeled the periphery of large spherical structures likely representing nuclei (Fig. 1B and C and Movie S1), as was corroborated by staining cells with

4′,6-diamidino-2-phenylindole (DAPI) (Fig. 1D and E). Finally, we found that the ER arrangement in narrow hyphae branching from distal regions of mycelia was characterized by prominent cortical ER strands interconnected with the NE by a number of short cytoplasmic strands (Fig. 1E).

***P. anserina* possesses three proteins of the reticulon and Yop1 families.** Next, we searched for the genes potentially coding for proteins of the reticulon and Yop1 families in the *P. anserina* genome (52), and we identified one reticulon (*RTN1*) and two Yop1 (*YOP1* and *YOP2*) protein-encoding genes. The predicted RTN1 and YOP1 proteins possess characteristic RHD (Pfam02453) and TB2/DP1, HVA22 family (Pfam03134) domains, respectively. In contrast, YOP2 possesses an atypical N-terminal TB2/DP1, HVA22 domain, which bears only one transmembrane domain in its first hydrophobic segment (Fig. S2).

YOP2 localizes to distinct ER domains and is enriched in the apical ER subcompartments. A search for YOP1 orthologues in fungal genomes identified *S. cerevisiae* Yop1p as the orthologue of *P. anserina* YOP1. In contrast, we did not identify orthologues of *YOP2* in most Saccharomycotina fungi (with the exception of *Yarrowia lipolytica*). Nonetheless, *YOP2* orthologues were present throughout filamentous ascomycetes (Pezizomycotina), as well as in most basidiomycete fungi (Agaricomycotina and Pucciniomycotina), and in selected sequenced genomes available for early-diverging fungi (Blastocladiomycota, Chytridiomycota, and Mucormycota). These observations indicate a wide distribution for *YOP2* in fungi; nonetheless, no YOP2 protein has been previously characterized. Therefore, we first sought to define whether *P. anserina* YOP2 actually localizes to the ER. We generated strains expressing an mCherry C-terminally tagged version of YOP2 by tagging the *YOP2* gene at its chromosomal location. YOP2-mCherry exhibited dim fluorescence; therefore, by the same strategy we also generated strains expressing GFP-tagged YOP2. We did not observe growth or developmental defects in the strains expressing the YOP2 tagged proteins. YOP2-GFP exhibited a polarized distribution in hyphae, with higher fluorescence intensity in the apical region (Fig. 2A and B and Movie S2). In this region, YOP2-GFP predominantly localized to a number of pleomorphic patches (Fig. 2A, arrows) similar to the apical ER subcompartments labeled by ER-GFP. In subapical cells, YOP2-GFP localized to a network of strands, which were similar to those labeled by ER-GFP but more discontinuous and limited in extension (Fig. 2A and C). In addition, YOP2-GFP localized to the cortical ER (Fig. 2D) and faintly labeled the NE with a patchy distribution (Fig. 2E). Despite its weak fluorescence, YOP2-mCherry colocalized with ER-GFP at both the apical patches (Fig. 2F) and subapical strands (Fig. 2G) in double-label experiments. These observations indicate that YOP2 resides in different domains of the ER, with a prominent localization in the apical ER subcompartments.

RTN1 localizes to the peripheral ER and is enriched in the apical ER subcompartments. Next, we studied the localization of RTN1 by generating strains expressing a GFP C-terminally tagged version of RTN1 by tagging the *RTN1* gene at its native locus. These strains exhibited the wild-type phenotype, including normal ascospore formation in homozygous crosses (Fig. S3; note that ascospore formation is affected in *rtn1* mutants; see below), indicating that RTN1-GFP is a functional protein. We found that, similarly to YOP2, RTN1-GFP exhibited a polarized localization in hyphae with increased fluorescence in the apical region (Fig. 3A and B and Movie S3), where it predominantly localized to the apical ER subcompartments (arrows). In subapical hyphal regions, RTN1-GFP less strongly labeled peripheral ER strands (Fig. 3C), including strands of the cortical ER (arrowhead). RTN1-GFP also labeled short strands in the vicinity of nuclei (Fig. 3D), but no distinctive NE labeling by RTN1-GFP was observed.

RTN1-GFP associates with the Spitzenkörper. In addition to the peripheral ER, we found that an apical punctum located at the hyphal tip was strongly stained by RTN1-GFP (Fig. 3A and Fig. 4A). This structure displayed poleward movement, which correlated with the extension of the hyphal tip (Movie S3), and its dynamics was reminiscent of the Spitzenkörper, a dynamic apical body conducting hyphal polar growth and

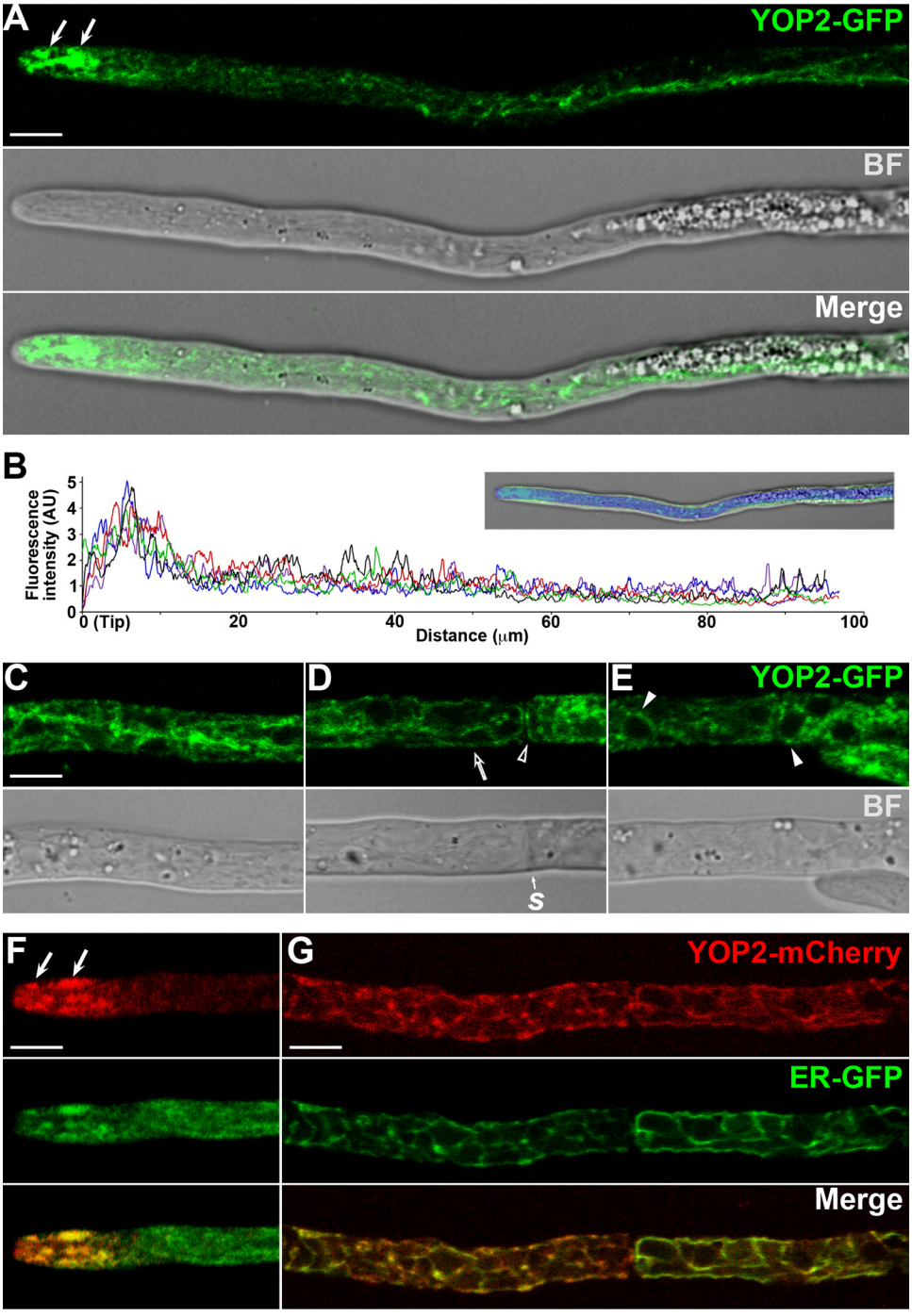

FIG 2 Localization of YOP2 in vegetative hyphae. (A) Localization of YOP2-GFP in the apical segment of growing leading hypha of young mycelial cultures. (B) Line scan graph of the fluorescence intensity profile of YOP2-GFP along growing leading hyphae; each line represents the line scan of an independent hypha. The upper panel shows an example of the line scan (blue) used to determine the intensity profile. (C to E) YOP2-GFP localization in distal regions of leading hypha. Note that the imaging parameters were optimized for YOP2-GFP detection in these regions and differ from panel A. (F and G) Localization of YOP2-mCherry and ER-GFP in apical (F) and distal (G) regions of hyphae. Arrows point to apical ER subcompartments, arrowheads to the nuclear envelope, open arrows to cortical ER, and open arrowheads to cortical ER bordering septa (*s*). BF, bright field; AU, arbitrary units. Bar, 5 μm.

morphogenesis. The Spitzenkörper is proposed to act as a vesicle supply center, which concentrates vesicles that transport cell wall-synthesizing enzymes for their subsequent delivery to the apical membrane, facilitating localized cell surface expansion at the hyphal tip (53, 54). We analyzed the Spitzenkörper by staining growing cells with

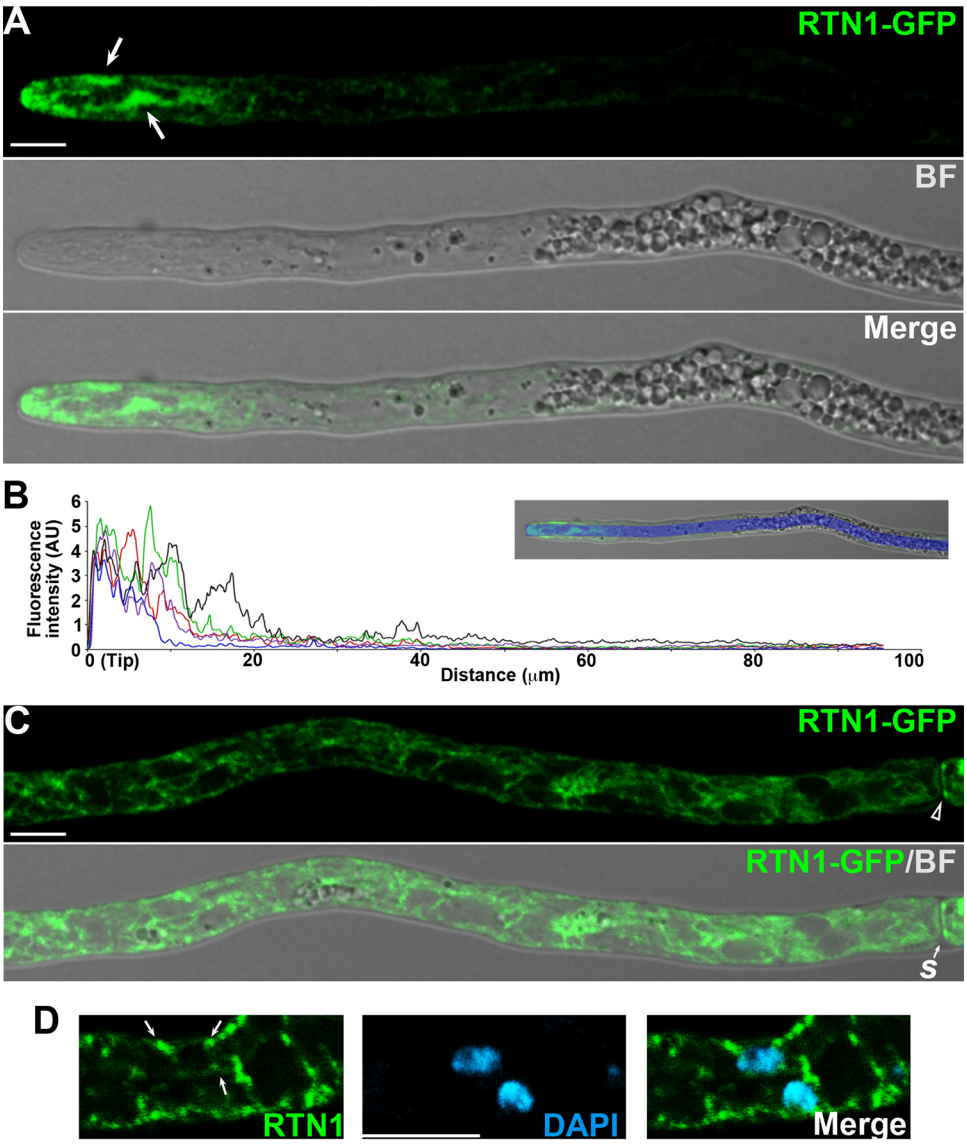

FIG 3 Localization of RTN1 in vegetative hyphae. (A) RTN1-GFP localization in the apical region of growing leading hyphae of young mycelial cultures. Arrows point to apical ER subcompartments. (B) Line scan graph of the fluorescence intensity profile of RTN1-GFP along growing leading hyphae; each line represents the analysis of an independent hypha. The upper panel shows an example of the line scan (blue) used to determine the intensity profile. (C) RTN1-GFP localization in the distal region of a leading hypha. The open arrowhead shows the cortical ER bordering septa (*s*). Note that to enhance RTN1-GFP detection, the imaging parameters differ from panel A. (D) Localization of RTN1-GFP in relation to nuclei (DAPI). Small arrows point to ER strands neighboring nuclei. BF, bright field; AU, arbitrary units. Bar, 5 μm.

FM4-64—a lipophilic fluorescent dye that labels this structure (54)—and found that RTN1-GFP was associated with the Spitzenkörper (Fig. 4B and C). The presence of the Spitzenkörper in a living hypha is associated with its elongation, and its position at the apex correlates with the hyphal growth direction. Actually, we observed that the appearance and disappearance events, and the changes in position of the FM4-64-stained Spitzenkörper, which were associated with hyphal growth and directionality, were mirrored by RTN1-GFP tip localization (Movie S4), corroborating its dynamic association with the Spitzenkörper. To rule out that the Spitzenkörper localization of RTN1 was artificially produced by the C-terminal tagging, we also analyzed the localization of a GFP N-terminally tagged version of RTN1. For this, we ectopically expressed a *GFP*::*RTN1* gene in cells deleted for the *RTN1* gene (Δ*rtn1*, see below). GFP-RTN1 was able to

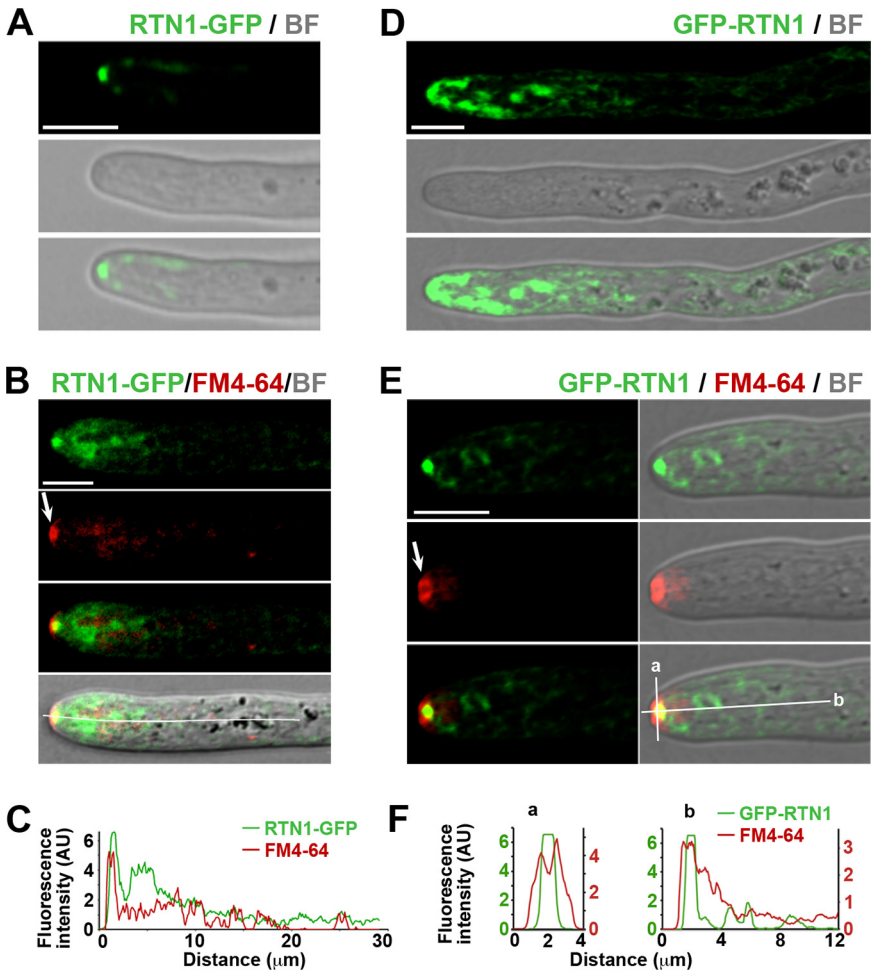

FIG 4 RTN1 localizes to the Spitzenkörper. Apical localization of RTN1-GFP (A) and compared localizations of RTN1-GFP and the FM4-64-stained Spitzenkörper (B) in growing leading hyphae of young mycelial cultures. (C) Fluorescence intensity profile of RTN1-GFP and FM4-64 along the hypha depicted in panel B (white line). (D and E) Localization of GFP-RTN1 expressed in a Δ*rtn1* growing leading hypha (D) and compared apical localizations of GFP-RTN1 and the FM4-64-stained Spitzenkörper (E). (F) Fluorescence intensity profile of GFP-RTN1 and FM4-64 along the lines depicted in panel E, lines a and b, respectively. Note that the imaging parameters of panel D were enhanced to detect GFP-RTN1 at the apical subcompartments. Arrows point to the Spitzenkörper. BF, bright field; AU, arbitrary units. Bar, 5 μm.

complement the Δ*rtn1* ascospore formation defects (Fig. S3), corroborating that this version of RTN1 is also functional. GFP-RTN1 showed the same characteristic distribution of RTN1-GFP, including its prominent localization at the apical ER subcompartments and at the Spitzenkörper (Fig. 4D to F and Movie S5). In addition, we observed that GFP-RTN1 displayed this same localization pattern when *GFP*::*RTN1* was expressed in the wild-type (*RTN1*$^+$) genetic context (Fig. S3 and Movie S5). Of note, we observed that, in contrast to the annular appearance of the FM4-64-stained Spitzenkörper, RTN1 localized to a discrete punctum of this structure (Fig. 4B, C, E, and F and Fig. S3), denoting that it localizes to the Spitzenkörper core.

The mycelial growth is moderately reduced in the absence of RTN1, YOP1, and YOP2. Next, we studied the function of YOP1, YOP2, and RTN1 by generating strains deleted for their corresponding genes. First, we observed that the *P. anserina* mycelial growth on standard dextrin-based medium was not significantly affected by the elimination of either of these genes (Fig. 5A to C). Then, we generated double and triple mutant strains deleted for these genes in all different combinations, and we observed a slight mycelial growth rate reduction in the double mutants involving Δ*yop1* (Δ*yop1*

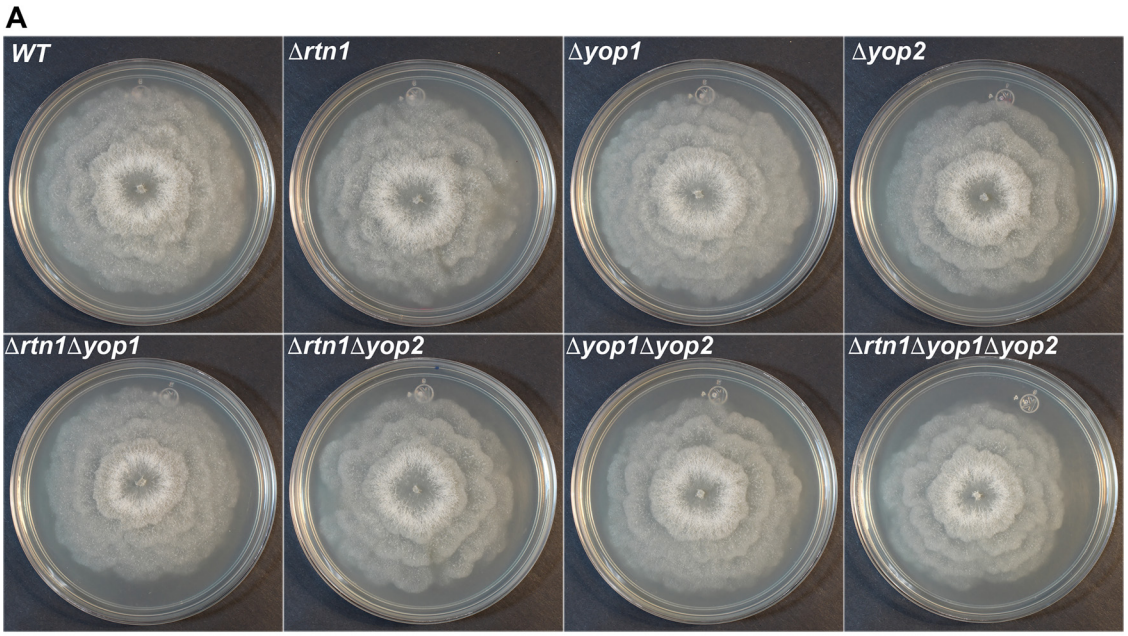

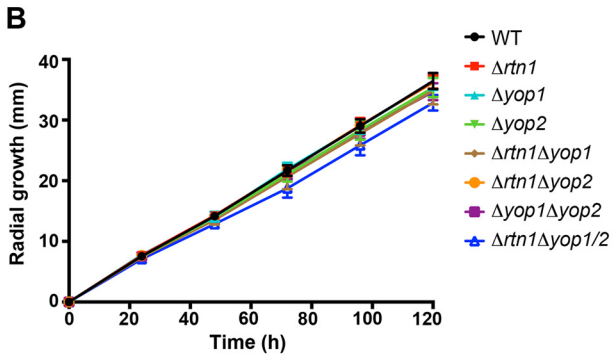

C

Strain	Growth rate (μm / h)	Sig. *P*-value
WT	302.5 ± 2.7	-
Δrtn1	301.3 ± 2.6	>0.9999
Δyop1	301.5 ± 3.2	>0.9999
Δyop2	293.2 ± 3.5	0.1883
Δrtn1Δyop1	288.8 ± 5.0	0.0209
Δrtn1Δyop2	301.1 ± 2.5	>0.9999
Δyop1Δyop2	289.0 ± 3.1	0.0235
Δrtn1Δyop1Δyop2	269.5 ± 3.8	<0.0001

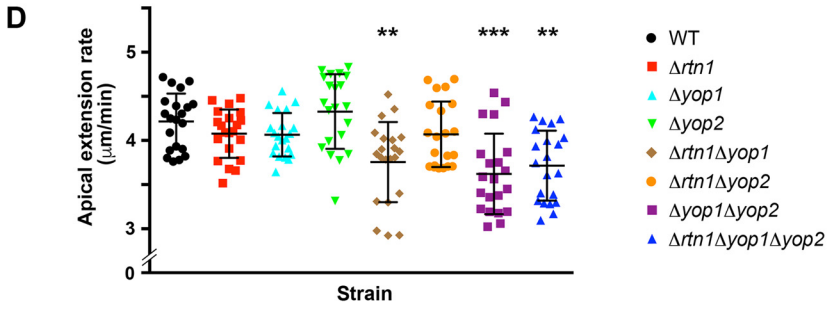

FIG 5 Growth phenotypes of *P. anserina* strains deficient for ER-shaping proteins. Mycelial growth of wild-type (WT) and deletion mutant strains deficient for the ER-shaping proteins RTN1, YOP1, and/or YOP2 on dextrin-containing medium. (A) Colonial growth at 120 h. (B) Growth curves. Values are mean ± SD from three independent experiments per strain, each with triplicates. (C) Growth rates of the strains analyzed in panel B; values are mean ± SEM. Statistically significant differences were evaluated by two-way ANOVA using a Tukey *post hoc* test; the adjusted *P* values of the mutant strains against the wild type are presented (Sig.). (D) Quantification of the apical extension rate of individual growing leading hyphae of the indicated strains. Scatterplots show the mean ± SD; $n = 21$ hyphae (from 3 independent experiments; 7 hyphae/experiment). **, $P < 0.01$; ***, $P < 0.0001$ relative to the WT by two-way ANOVA with Tukey's *post hoc* test.

Δ*yop2* and Δ*rtn1* Δ*yop1* [Fig. 5]), as well a moderate reduction (i.e., ≈10%) in the Δ*rtn1* Δ*yop1* Δ*yop2* triple mutant, compared to the wild type (Fig. 5A to C). In addition, we evaluated the effect of *RTN1*, *YOP1*, and *YOP2* deletion on the growth of individual hyphae. We analyzed the apical extension rate of growing leading hyphae by live-cell imaging and found that, similar to mycelia, it was not significantly affected by the

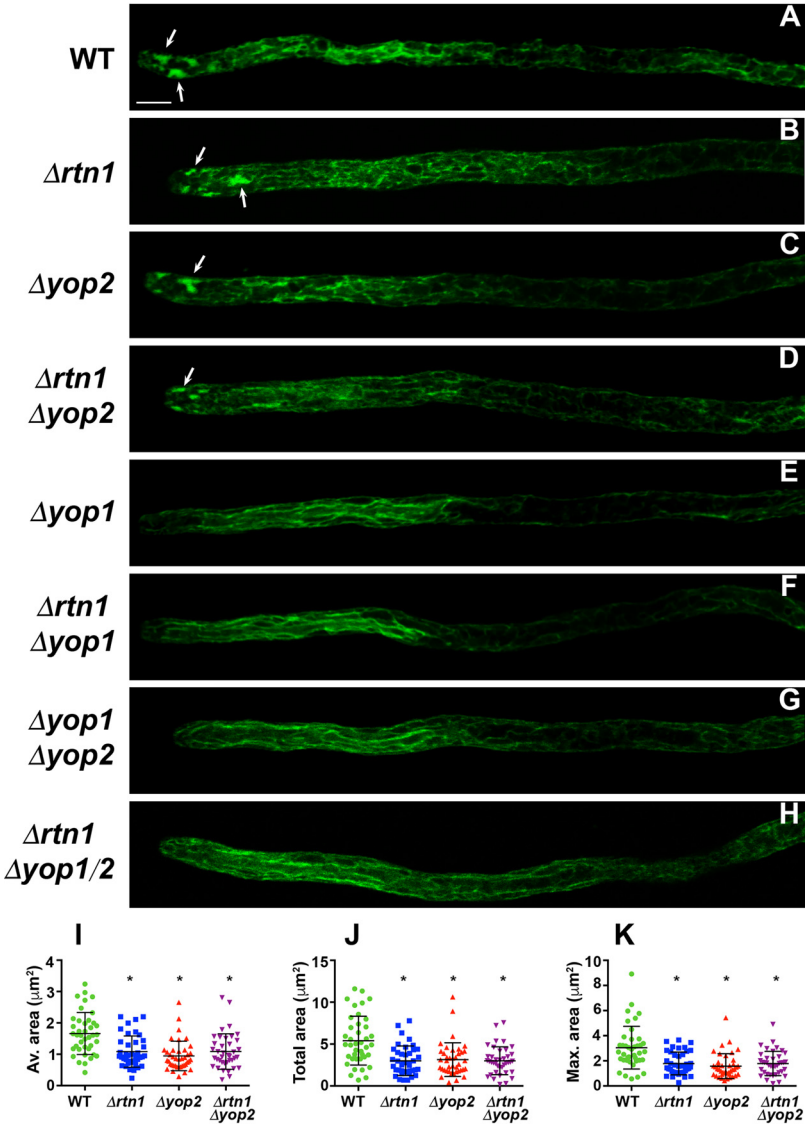

FIG 6 YOP1, YOP2, and RTN1 are required for ER shaping. (A to H) Analysis of ER-GFP-labeled ER in the apical region of growing leading hyphae of young mycelial cultures of strains of the indicated genotypes (WT, wild type). Arrows point to apical ER subcompartments. Bar, 5 μm. (I to K) Quantification of the average area of the apical subcompartments per hypha (I), of the total area occupied by all apical subcompartments in a hypha (J), and of the maximal area attained by an apical subcompartment per hypha (K) of WT, Δ*rtn1*, Δ*yop2*, and Δ*rtn1* Δ*yop2* strains. Scatterplots show the mean ± SD; n = 40 hyphae (from 4 independent experiments; 10 hyphae/experiment). *, $P < 0.0001$ relative to the WT by two-way ANOVA with Tukey's *post hoc* test.

single elimination of either RTN1, YOP1, or YOP2 (Fig. 5D). Nonetheless, we observed a moderate reduction in the apical extension rate of Δ*yop1* Δ*yop2* (average 3.62 ± 0.5 μm/min), Δ*rtn1* Δ*yop1* (average 3.76 ± 0.5 μm/min), and Δ*rtn1* Δ*yop1* Δ*yop2* (average 3.71 ± 0.4 μm/min) mutant hyphae, compared to the wild type (average 4.21 ± 0.3 μm/min) (Fig. 5D). These observations suggest that the *P. anserina* reticulon and Yop1 proteins perform redundant functions required for optimal vegetative growth.

ER structure depends to different extents on RTN1, YOP1, and YOP2. We assessed the participation of YOP1, YOP2, and RTN1 in ER structuring by analyzing the localization of ER-GFP in the different deletion strains (Fig. 6A to H). We discovered that elimination of either RTN1 (Fig. 6B) or YOP2 (Fig. 6C) resulted in a decrease in the size of the apical ER subcompartments, relative to the wild type (Fig. 6A), as revealed by

determining the average (Fig. 6I), the total (Fig. 6J), or the maximal (Fig. 6K) area occupied by the apical ER subcompartments in hyphae of the corresponding deletion mutants. We did not observe additive defects or suppression of this phenotypic trait upon simultaneously eliminating RTN1 and YOP2 (Fig. 6D and I to K). Interestingly, we found that the elimination of YOP1 by itself generated a more severe defect in the formation of the apical ER subcompartments, which were virtually undetectable in the Δ*yop1* mutant (Fig. 6E). This defect was accompanied by a rearrangement of the peripheral ER of the subapical hyphal region, which was characterized by ER strands predominantly displaying a longitudinal arrangement and that appeared to be less branched (Fig. 6E). We found that Δ*yop1* was epistatic on Δ*rtn1* (Fig. 6F) and Δ*yop2* (Fig. 6G) for this phenotype and that the triple Δ*rtn1* Δ*yop1* Δ*yop2* mutant (Fig. 6H) displayed the same phenotype as the single Δ*yop1* mutant. These observations indicate that the formation of the apical ER depends to a different extent on the activity of YOP1, YOP2, and RTN1, where YOP1 exerts a major contribution.

The elimination of RTN1 affects sexual development. Then, we analyzed the effect of *YOP1*, *YOP2*, and *RTN1* deletion on sexual development. *P. anserina* is a heterothallic ascomycete that reproduces exclusively sexually. Sexual development takes place inside multicellular fructifications (perithecia), which enclose the sexual tissue (the hymenium) where karyogamy, meiosis, and ascospore (the meiosis-derived spore) formation occur. This process involves the formation of a specialized ascogenous hypha—the crozier—where opposite mating-type nuclei are compartmentalized in a dikaryotic cell. This cell undergoes karyogamy, enters meiosis, and differentiates into an ascus (the meiocyte). The ascus elongates along meiotic prophase-I, and after ending meiosis, a mitotic division yields eight haploid nuclei, which are enclosed by pairs into four ascospores. Although formally heterothallic, *P. anserina* usually produces dikaryotic ascospores, which possess opposite mating-type nuclei and upon gemination yield a heterokaryotic mycelium that is able to self-fertilize. This reproductive strategy is referred to as pseudohomothallism. Ascospore differentiation and maturation are completed inside the original ascus (Fig. S1) (55, 56).

First, we analyzed sexual development in sexual crosses homozygous for Δ*yop1*, Δ*yop2*, or Δ*rtn1*. We did not observe defects in the formation of perithecia in either genetic context, indicating that YOP1, YOP2, and RTN1 are not required for fertilization or perithecium formation. We also observed that perithecia issued from these crosses were able to produce ascospores (Fig. 7A to G), implying that YOP1, YOP2, and RTN1 are not strictly required for karyogamy, meiosis, or ascospore formation. Nonetheless, we observed that ascospores produced in Δ*rtn1* homozygous crosses were abnormal (Fig. 7D to G). We found that, in contrast to the wild type, which primarily produces asci containing four ascospores of even size (Fig. 7A), Δ*rtn1* perithecia frequently contained asci with ascospores of uneven sizes and in irregular numbers (Fig. 7D to G). Eventually, Δ*rtn1* asci containing a single gigantic ascospore were produced (Fig. 7E), as well as asci producing a single large banana-shaped ascospore (Fig. 7G). These asci were observed at a very low frequency in the Δ*rtn1* strain (i.e., in 0.6% of asci, $n = 1{,}200$ from 3 independent experiments); however, they were never observed in the wild type ($n > 1{,}200$). Overall, we found that around 40% (41% $\pm$ 4.2%) of asci issued from Δ*rtn1* homozygous crosses were abnormal, compared to less than 2% (1.5% $\pm$ 5.8%) in the wild type (Fig. 7H). These defects were not observed in heterozygous crosses of Δ*rtn1* to the wild type (Fig. 7H), indicating a recessive phenotype. This phenotype was also not observed in Δ*yop1*, Δ*yop2*, or Δ*yop1* Δ*yop2* homozygous crosses (Fig. 7B, C, and H), and it was not exacerbated or suppressed upon deleting *YOP1* and/or *YOP2* in the Δ*rtn1* context (Fig. 7H). Finally, we showed that the ectopic introduction of a wild-type allele of *RTN1* into the Δ*rtn1* genetic background restored ascospore formation (Fig. S3), corroborating that this phenotype was caused by *RTN1* deletion.

Ascospore germination is affected in the absence of RTN1. Next, we inspected whether ascospore germination was affected by RTN1 loss. We found that 86% of Δ*rtn1* ascospores ($n = 102$) were able to geminate when they were issued from morphologically normal Δ*rtn1* asci (i.e., asci containing 4 ascospores of even size),

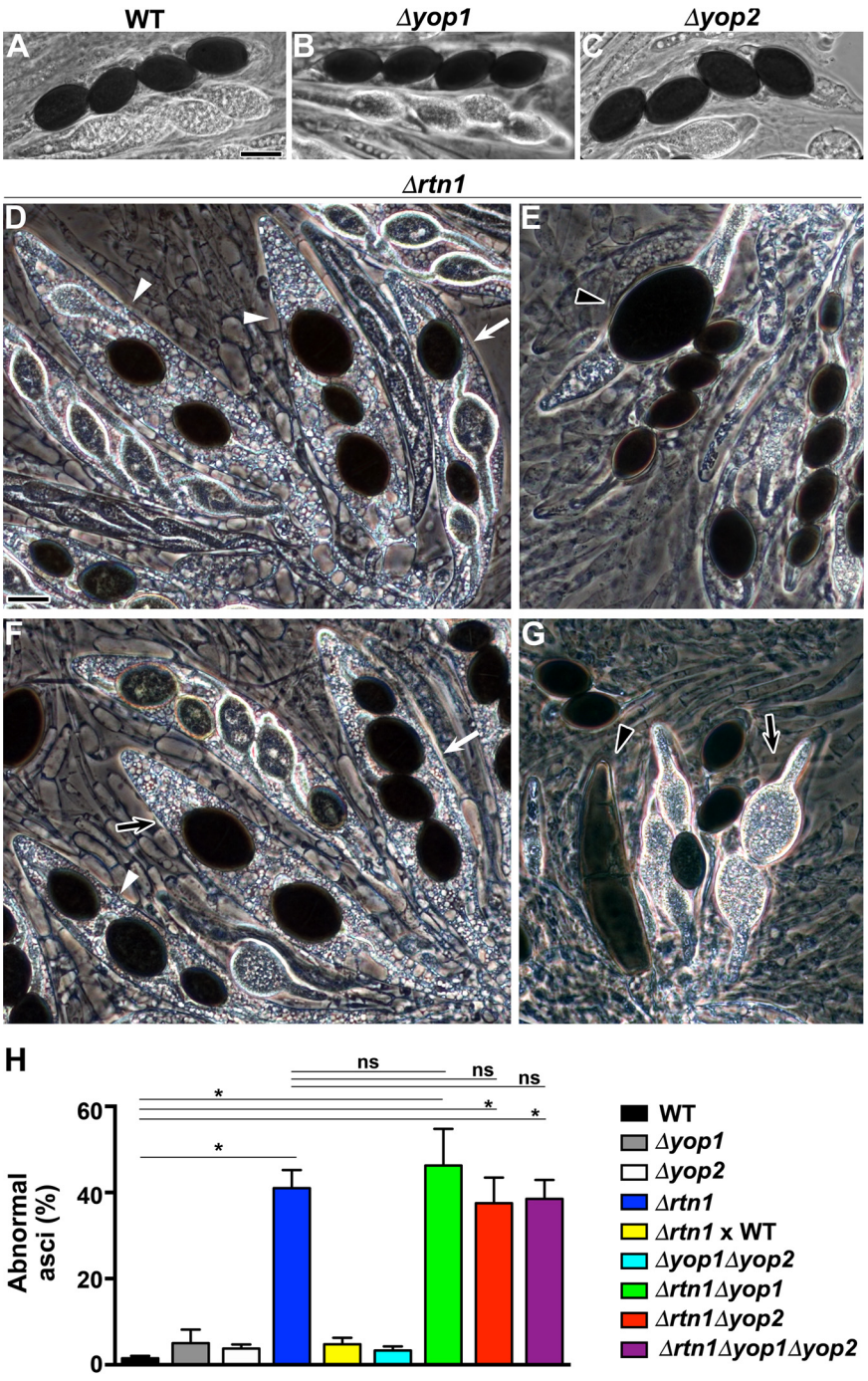

FIG 7 *RTN1* deletion affects ascospore formation. Asci issued from WT (A), Δ*yop1* (B), Δ*yop2* (C), and Δ*rtn1* (D to G) homozygous crosses. Note that in contrast to the WT, Δ*yop1*, and Δ*yop2* asci, which contain four ascospores of even size, Δ*rtn1* asci produce ascospores of uneven size (white arrows), in irregular numbers (black arrows; note an earlier developmental stage in panel G), and irregular in both size and number (white arrowheads). Eventually, Δ*rtn1* asci containing a single giant ascospore, as well as a large banana-like ascospore (black arrowheads in panels E and G, respectively), were produced. Bar, 20 μm. (H) Quantitation of abnormal asci in the indicated sexual crosses. Δ*rtn1* × WT corresponds to a heterozygous mutant × WT cross, and the remaining crosses correspond to homozygous crosses of the indicated genotypes (n = 400 asci from four independent experiments). *, $P < 0.0001$ by one-way ANOVA with Tukey's *post hoc* test; ns, not statistically significant.

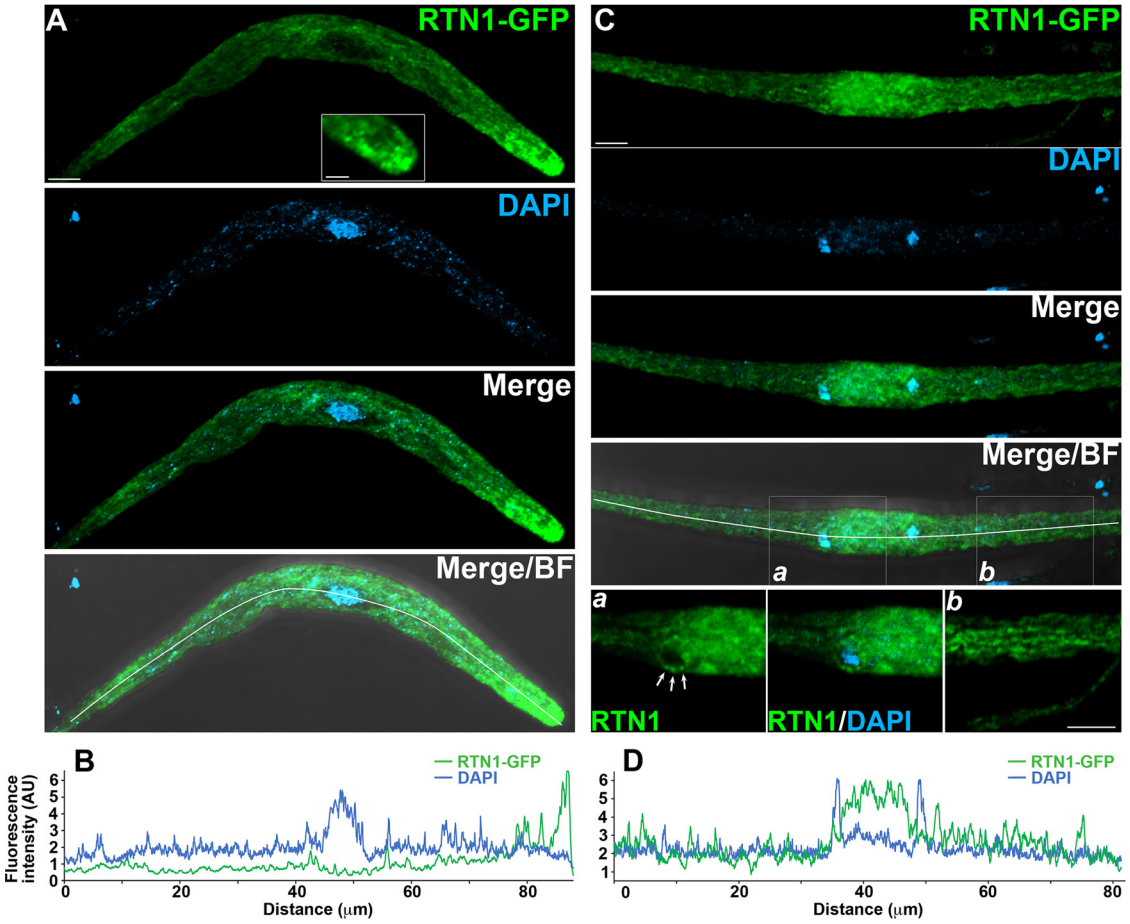

FIG 8 RTN1 localization is regulated during meiotic development. (A) RTN1-GFP localization in a late meiotic prophase-I ascus. The inset shows an enlarged single-plane micrograph of the ascus tip. (B) Line scan graph of the fluorescence intensity for RTN1-GFP (green) and DAPI (blue) channels along the ascus in panel A (white line). (C) RTN1-GFP localization in an ascus after the first meiotic division. Insets *a* and *b* display enlarged single-plane images of the corresponding boxed areas. In inset *a*, the localization of RTN1-GFP is compared to that of a nucleus (DAPI), and arrows point to RTN1-GFP foci at the nuclear periphery; inset *b* shows RTN1-GFP localization near the cell cortex. (D) Line scan graph of the fluorescence intensity for RTN1-GFP (green) and DAPI (blue) channels along the ascus in panel C (white line). Note the increase in RTN1-GFP fluorescence in the ascus middle region, which is bordered by the segregating nuclei. Except for the insets, images show maximum-intensity projections of z series through the entire cells. DNA was stained with DAPI. BF, bright field. Bars, 5 μm. Inset bar in panel A, 2 μm.

compared to 98% in the wild type (n = 102). We also found that the Δ*rtn1* germination rate was reduced to 55% when ascospores were issued from abnormal Δ*rtn1* asci (n = 102 ascospores). In these asci, we found no correlation between the ascospore size and its germination capacity (i.e., the germination rates for ascospores of regular and abnormal size were 44% and 56%, respectively). These findings show that RTN1 is required for ascospore germination, in correlation with its influence in ascus development.

RTN1 localization is regulated during meiotic development. Then, we analyzed the localization of RTN1-GFP during ascus development. Similar to vegetative hyphae, we found that RTN1-GFP displayed a polarized distribution early during ascus development, at the stages where asci elongate along meiotic prophase-I (Fig. 8A and B). In these asci, RTN1-GFP displayed increased fluorescence toward the apex, where it localized to a number of apical patches (Fig. 8A, inset). This suggests that RTN1 also associates with a specialized ER subdomain in the polarized growing regions of this specialized hyphal cell type. Following meiotic prophase-I, when the ascus reached its final length, the intensity of RTN1-GFP fluorescence at the apical region decreased concomitantly with an increase in ascus middle region. RTN1-GFP prominently localized to the

ascus middle region during meiotic progression, in the vicinity of the region where nuclei segregate (shown for an ascus after meiosis-I in Fig. 8C and D). Consistent with peripheral-ER localization, RTN1-GFP localized to a network of strands in these cells (Fig. 8C, inset *b*). However, we found that RTN1-GFP also localized to a number of small puncta bordering nuclei (Fig. 8C, inset *a*). These observations show that the localization of RTN1 is regulated during meiocyte development.

Loss of RTN1 affects nucleus segregation during meiotic development. In *P. anserina*, the defects in the number and size of ascospores produced in an ascus can result from defective meiotic nucleus segregation, which leads to uneven packaging of nuclei into ascospores. In this fungus, both meiotic divisions occur along the long axis of the ascus, resulting in four equally spaced nuclei upon meiosis completion (Fig. 9A). At the following interphase (interphase-II in Fig. 9A), each pair of second-division sister nuclei migrate toward each other, producing two pairs of nuclei placed at opposite sides of the ascus (Fig. 9B). These nuclei then undergo mitosis with a division plane perpendicular to the ascus long axis, which results in four pairs of closely associated nonsister nuclei (postmeiotic mitosis in Fig. 9A). Upon ascospore delineation, each of these pairs of nuclei becomes included within a common ascospore (Fig. 9A). As a result, most asci contain four even-sized binucleate ascospores (Fig. 9C). In a small percentage of asci (≈2%), one of the four binucleated ascospores produced is replaced by two small uninucleate ascospores (Fig. S1) (55–59).

We analyzed nuclear distribution in asci issued form Δ*yop1* (Fig. 9D), Δ*yop2* (Fig. 9E), and Δ*rtn1* (Fig. 9F to J) homozygous crosses. We found that the distribution of nuclei in Δ*rtn1* ascospores was uneven. Consistent with the ascospore formation defects of Δ*rtn1*, we observed that the number of nuclei of Δ*rtn1* ascospores was abnormal, in correlation with the size of the ascospores and with their number per ascus (Fig. 9H to J). In addition, we observed defects in the distribution of nuclei following meiosis (Fig. 9F) and the postmeiotic mitosis (Fig. 9G).

Loss of RTN1 affects spindle dynamics during meiotic development. Alterations in the distribution of nuclei in ascospores in *P. anserina* can be produced by defective spindle positioning or impaired nuclear migration during meiotic development (59–61). In this fungus, the spindles are positioned along the long axis of the ascus during both meiotic divisions (shown for meiosis-I in Fig. 10A), whereas they are perpendicular to it at postmeiotic mitosis, where they are placed as two parallel pairs at opposite sides of the cell (Fig. 10B and Movie S6) (57, 58). We analyzed spindle arrangement during meiotic development and found that *RTN1* deletion produced defects in spindle orientation during both meiotic divisions (Fig. 10C and D) and postmeiotic mitosis (Fig. 10E and F and Movie S6). We also observed altered spindle positioning during postmeiotic mitosis, with spindles randomly scattered in the ascus instead of being widely separated as parallel pairs (Fig. 10F). In addition, we found defects in spindle morphology, which could reflect defective spindle assembly (Fig. 10F and G, arrows), as well as genetic material likely representing chromosomes, which were not associated with detectable spindles (Fig. 10C, D, and G, asterisks). Overall, we observed that 61.8% of Δ*rtn1* asci ($n = 34$) displayed spindle arrangement abnormalities at either the meiotic (in 60% of asci, $n = 20$) or postmeiotic (in 64.3% of asci, $n = 14$) divisions, compared to 9.5% in the wild type (12% at meiosis, $n = 25$; 5.9% at postmeiotic mitosis, $n = 17$). These results show that spindle dynamics during *P. anserina* meiotic development requires RTN1.

DISCUSSION

Here, we analyzed the function of the proteins of two main families of ER-structuring proteins—the reticulon and Yop1/DP1 families—during development of the model fungus *P. anserina*. We found that this fungus possesses three proteins of these families and found that they perform partially redundant roles during its vegetative (somatic) phase. In addition, we discovered that one of these proteins—the reticulon RTN1—is distinctively required during sexual development. This protein associates with different domains of the ER at different developmental stages, where it likely participates in

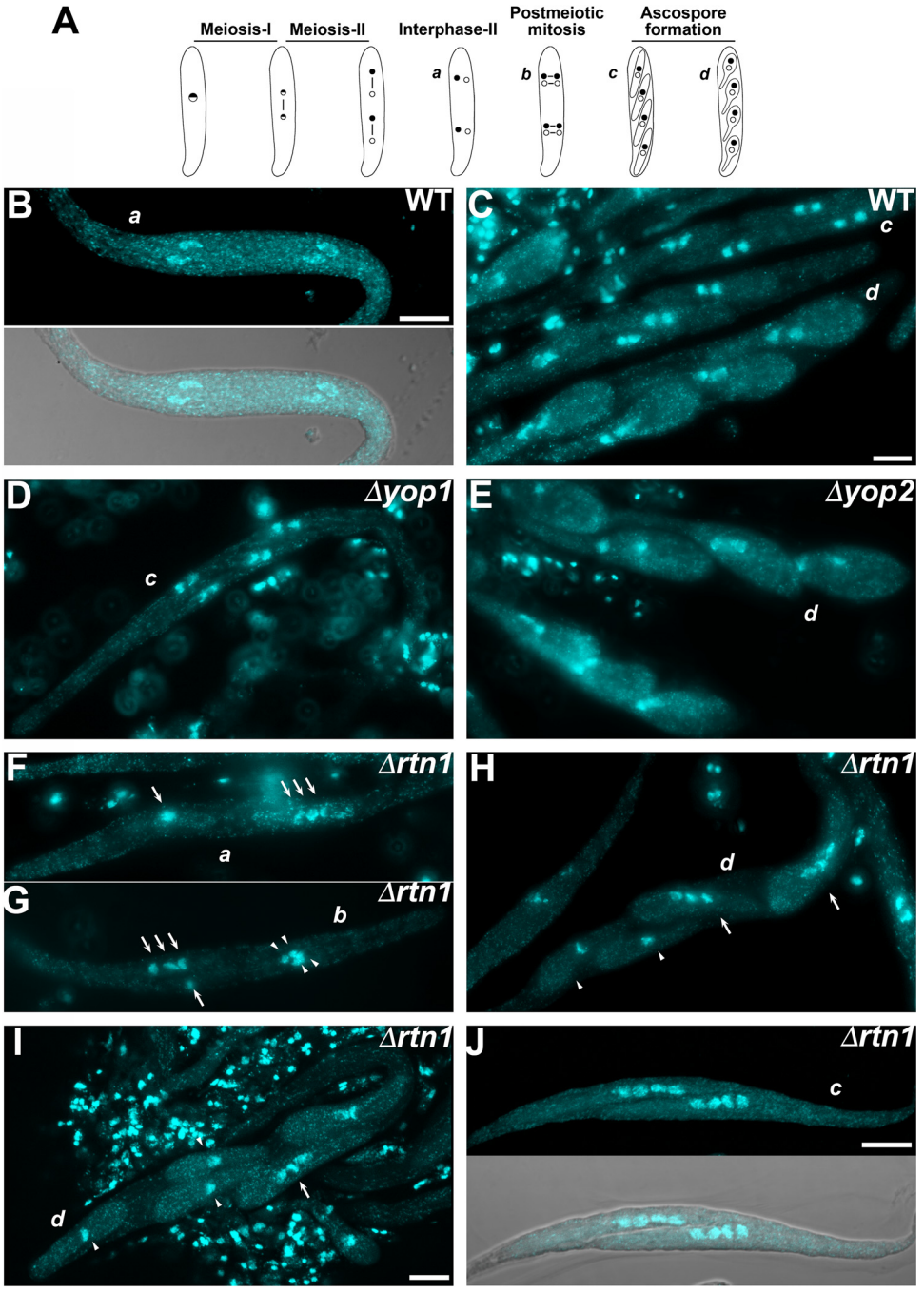

FIG 9 *RTN1* deletion affects the segregation of nuclei during meiotic development. (A) *P. anserina* meiotic development from late prophase-I to ascospore formation (from left to right). Dots represent nuclei, and the lines connecting dots represent spindles (see the text for details). Small lettering indicates successive developmental stages shown in the figure. (B to J) Nucleus distribution during meiotic development of WT (B and C), Δ*yop1* (D), Δ*yop2* (E), and Δ*rtn1* (F to J) homozygous crosses. Wild-type meiosis results in four evenly distributed nuclei, which associate as pairs at the following interphase (B) to then divide across the ascus. This produces four pairs of nuclei, which are packaged into four ascospores (C; three asci at progressive developmental stages, from top to bottom, are seen, each containing four binucleate ascospores). Δ*yop1* (D) and Δ*yop2* (E) asci exhibited normal meiotic nucleus distribution. Δ*rtn1* asci displayed alterations in the disposition of nuclei following meiosis (F; note the three clustered nuclei distant from a single isolated nucleus [arrows]; compare to panel B), at postmeiotic mitosis (G; note the three clustered nuclei next to a single nucleus [arrows], compared to two pairs of nuclei [arrowheads] at the opposite side of the ascus), and in ascospores (H to J; compare to panel C). Note that the abnormal meiotic nucleus disposition of panel F could yield an ascus with the uneven ascospore nuclear distribution of panel H. Also note the two tetranucleate ascospores in panel J, which upon growth and maturation could develop into the two large ascospores shown in Fig. 7G and F (black arrows), respectively. DNA was stained with DAPI. Lower panels in panels B and J show DAPI/bright-field merge images. Bars, 5 μm.

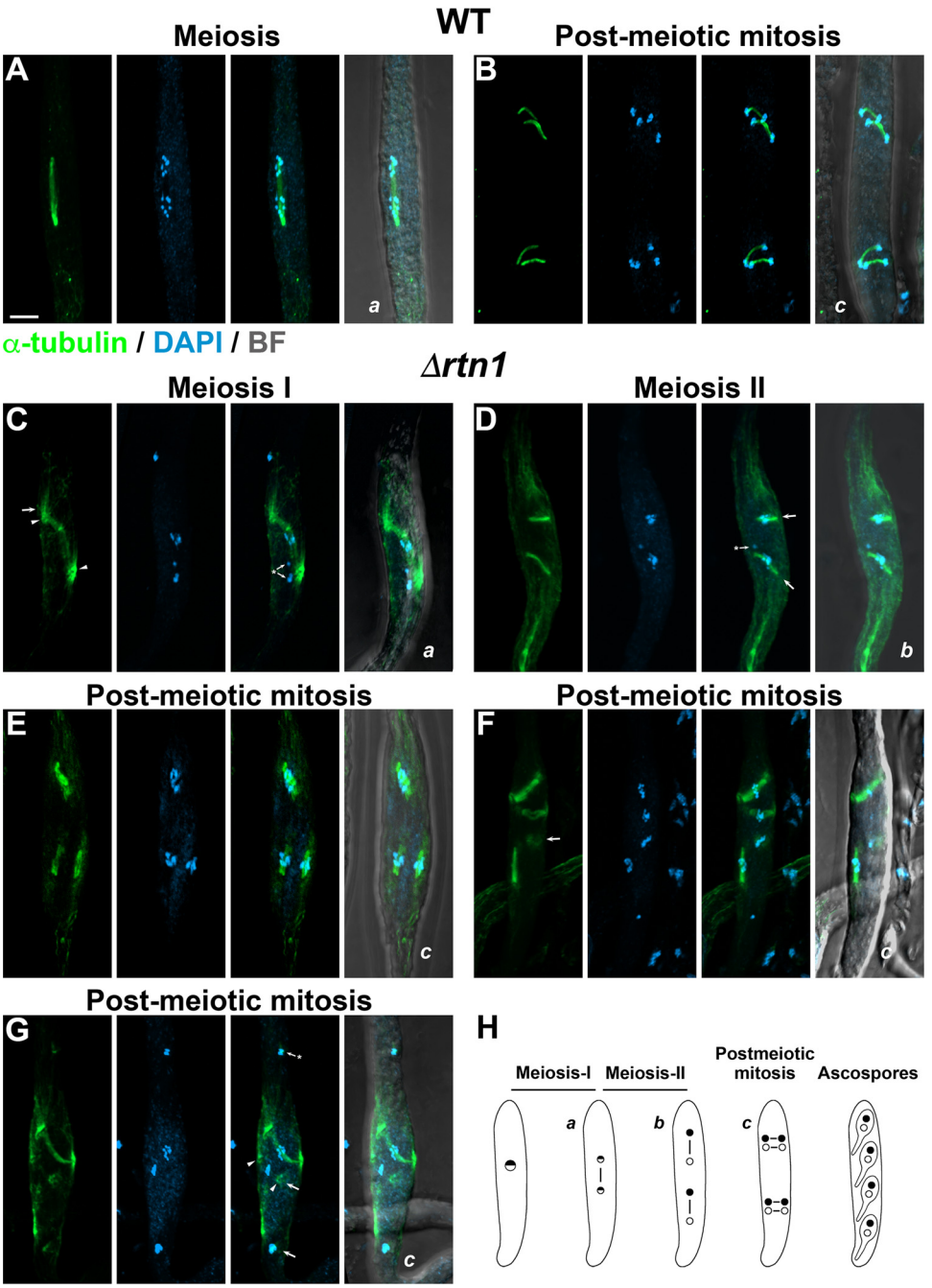

FIG 10 *RTN1* deletion affects spindle dynamics during meiotic development. Analysis of spindle arrangement during wild-type (A and B) and Δ*rtn1* (C to G) meiotic development. (H) Schematics of spindle positioning during wild-type meiotic development. (A) Wild-type meiosis (anaphase-I) showing the spindle longitudinally oriented along the ascus. Note the 14 chromosomes (n = 7) migrating toward the poles. (B) WT postmeiotic mitosis (telophase) showing the spindles positioned across the ascus and aligned in pairs at opposite sides of the ascus (see Movie S6 for a 3D reconstruction). (C) Δ*rtn1* first meiotic division (anaphase-I) with altered spindle positioning. Note the large array of astral microtubules (arrow; arrowheads point to the spindle poles) and the chromosomes not associated with the spindle (asterisk). (D) Δ*rtn1* second meiotic division (metaphase-II) with incorrect spindle orientation (arrows); note that one spindle is perpendicular to the ascus long axis, whereas the second one is oblique. Note also a chromosome not placed in the spindle (asterisk). (E to G) Δ*rtn1* postmeiotic mitosis asci. In panel E, the orientation of the four spindles is longitudinal instead of perpendicular to the ascus (note that the two upper spindles overlap; see Movie S6). In panel F, the spindles are randomly oriented and scattered along the ascus. Note also that one spindle is abnormal in shape (arrow). In panel G, one oblique spindle is observed, and a second is faintly detectable (arrows; arrowheads point to the spindle poles). The remaining two groups of chromosomes have no assembled spindles associated (small arrows). Asci in panels E to G are in metaphase. Images show maximum-intensity projections of z series through the entire cells. Small lettering indicates successive developmental stages. BF, bright field. Bar, 5 μm.

different developmental processes. Our research provides relevant information on the specific mechanisms involved in ER regulation during development.

We identified three proteins of the reticulon and Yop1 families in *P. anserina* and showed that two of them—RTN1 and YOP2—prominently localize to the apical domain of the peripheral ER, while the third one—YOP1—is required for its formation. To a lesser extent, RTN1 and YOP2 were also required for the formation of this domain. This ER domain specifically associates with the polarized growing region of hyphae (47); however, our finding that the formation of this domain depends on YOP1 but that no hyphal growth defect was produced upon its elimination argues against a role for this domain in polarized hyphal growth. Nonetheless, a moderate reduction in the apical extension rate of hyphae was observed when YOP1 was eliminated in combination with RTN1 and/or YOP2, and this defect was reflected in the mycelial growth. Yet, in this case, a stronger impact was observed when the three proteins were missing, which could indicate a different arrangement of the mycelial network of the distinct mutants. These observations suggest that these proteins perform overlapping functions required for ER integrity beyond solely shaping the apical ER compartments and indicate that these functions are required for optimal vegetative growth. Still, the growth reduction observed upon elimination of these proteins was moderate, which likely reflects additional proteins involved in structuring the ER. Actually, the growth of *S. cerevisiae* is also only partially reduced upon simultaneously eliminating its Yop1 and reticulon (Rtn1 and Rtn2) proteins (14), and an enhanced growth defect is produced when the Lunapark family protein Lnp1 is further disrupted (62).

We also discovered that a fraction of RTN1 associates with the Spitzenkörper. The Spitzenkörper is a complex structure localized at the tip of growing hyphae, which orchestrates the polarized traffic of cell wall-building vesicles and determines hyphal growth and morphogenesis. This structure accumulates secretory vesicles before being transported to the foremost apical membrane, supplying membrane lipids and cell wall-synthesizing enzymes at the expanding hyphal tip (53, 63). As shown in *Neurospora crassa*, where the Spitzenkörper comprises an outer layer of glucan synthase-containing macrovesicles surrounding a core of microvesicles transporting chitin synthases, this structure accommodates distinct secretory vesicles in different strata and could regulate their differential trafficking and sorting (63–65). These vesicles are subsequently delivered to the apical plasma membrane, where the exocyst complex mediates their localized exocytosis (66). In *P. anserina* RTN1 distinctly associated with a Spitzenkörper layer likely representing the microvesicle core. It is therefore possible that RTN1 is involved in the formation and/or trafficking of some of these vesicles. In line with this hypothesis, reticulons are required for the organization of the ER exit sites, regulate protein ER exit, and contribute to ER-Golgi trafficking (26, 27, 67). Moreover, reticulons promote exocytosis by enhancing the ER-to-the cell surface trafficking (25), and they interact with exocytic SNAREs (68). Furthermore, in *S. cerevisiae* Rtn1 interacts with the exocyst by directly binding to its subunit Sec6 (69), which could indicate a second association of reticulons with the polar growth apparatus of fungal cells. Interestingly, proteins involved in the regulation of autophagy localize to the Spitzenkörper in *Aspergillus nidulans*, where they could locally modulate autophagy to regulate secretion levels (70, 71). Reticulons play different functions in autophagy, including roles in autophagosome formation (72) and ER turnover by selective autophagy (34–37). It is therefore tempting to speculate that RTN1 is involved in an autophagy-related secretory system, which could regulate secretion to modulate the cell surface membrane supply and/or cope with excess ER (73, 74). These observations suggest a role for RTN1 in the tip growth apparatus of *P. anserina*. Our finding that no growth defect was observed in *RTN1*-deleted strains could indicate redundant components involved in this role.

The RTN1 apical localization during early meiotic development suggests that it could also participate in the tip growth apparatus of asci. Notably, RTN1 redistribution to the ascus middle region following ascus growth could indicate that it performs

different functions in distinct cell regions at different stages of ascus development. In the latter cell region, RTN1 could be involved in meiotic nucleus segregation, as supported by the finding that this process is compromised when RTN1 is missing. These observations also indicate that the ER undergoes a developmental remodeling during meiotic development. Interestingly, in contrast to the vegetative phase, where RTN1 seems to be partially redundant with YOP1 and YOP2, the latter proteins do not appear to be involved in meiotic development. Notably, no ascospore formation defects were observed in the plant-pathogenic fungus *Fusarium graminearum* upon disruption of the atlastin Sey1—a dynamin-like GTPase that mediates the fusion between the ER tubules, which generates the ER reticular network (75). These observations could indicate a specific role for RTN1 in meiotic development. Still, further research is required to elucidate the functional conservation of the ER-shaping proteins among fungi.

Our data support a role for RTN1 in the regulation of meiotic spindle dynamics. However, the precise participation of this protein in this process remains to be determined. RTN1 could be required for the organization of the NE during meiosis. In *P. anserina*, as in other ascomycetes, the NE is maintained during both meiotic divisions and postmeiotic mitosis (58). In *Schizosaccharomyces pombe*, meiosis involves a transient loss of the nucleocytoplasmic barrier, which occurs without NE breakdown (76–78), whereas the closed mitosis of *A. nidulans* involves extensive remodeling of the nuclear pore complexes, which changes their transport properties and allows timely access of tubulin and regulatory proteins to the nucleus (79, 80). Nuclear pore complexes insert into the NE at the sites where the outer and inner nuclear membranes are contiguous through highly curved membrane connections. Actually, the assembly and integrity of the nuclear pore complexes in the NE depend on the ER membrane-bending proteins (23, 81). Meiotic development in *P. anserina* could involve a remodeling of the nuclear pore complexes, requiring RTN1 and regulating the nuclear transport of proteins involved in spindle assembly and dynamics. In agreement with this hypothesis, we observed that a fraction of RTN1 localized to the nuclear periphery during meiotic development.

RTN1 might also be required for proper SPB functioning. The SPBs are microtubule-organizing centers, which are embedded in the NE and consist of two faces—facing the nucleoplasm and the cytoplasm, respectively—that serve as sites of nucleation for the spindle and the cytoplasmic microtubules, respectively (82). Nuclear distribution and spindle orientation in fungi rely on dynamic interactions and pulling forces exerted from the cell cortex on the cytoplasmic astral microtubules generated from the SPBs (83). Similar to the nuclear pore complexes, the SPBs insert into the NE at the sites where the outer and inner nuclear membranes fuse, in a process dependent on the ER membrane-bending proteins (28). In *S. cerevisiae*, loss of Rtn1 and Yop1 produces defects in SPB integrity, stability, and function, which result in reduced cytoplasmic microtubules and defective mitotic spindle formation. These defects lead to alterations in spindle structure, positioning, and orientation during mitosis (28). Therefore, in *P. anserina* RTN1 could be involved in promoting the assembly and stability of the SPBs during meiotic development.

In addition to microtubule assembly, the SPB plays a primordial role in ascospore formation. In *S. cerevisiae*, the SPB cytoplasmic face is transformed after meiosis from the site of microtubule nucleation into the vesicle docking complex (the meiosis-II outer plaque), which drives the assembly of the membrane that delineates ascospores (for review, see reference 84). In *P. anserina*, as in other Sordariales, rearrangements of the SPBs associated with ascospore formation occur following postmeiotic mitosis (57, 58, 85). Further supporting a role for RTN1 in SPB function, a number of Δ*rtn1* asci produced a single banana-shaped ascospore. Similar aberrant ascospores previously described in related fungi result from the formation of a single large ascospore wall beneath the ascus wall, which encloses all meiotic nuclear products (86). The formation of these ascospores is associated with SPB abnormalities (86) and could result from failure of the SPBs to conduct ascospore membrane formation around meiotic nuclei.

Altogether, our results show that the ER is subject to a developmental remodeling during sexual development, which involves the reticulon RTN1 and is required for proper progression of the sexual cycle. These findings add meiotic development to the number of developmental processes that rely on the activity of the ER-shaping proteins and underscore the relevance of the processes involved in shaping the ER in the regulation of cell development.

MATERIALS AND METHODS

Strains and culture conditions. The strains used in this investigation are derived from the *P. anserina* "S" wild-type strain, and all analyzed strains were homokaryotic. Homologous recombination gene targeting was done in the *P. anserina* Δ*ku70* strain (87). *P. anserina* was grown on M2 minimal medium containing 1.1% dextrin as sole carbon source, and protoplasts were regenerated on RG medium. Ascospores were germinated in G medium supplemented with yeast extract (0.5%). After 36 to 48 h of growth at 27°C, mycelial explants from the center of the resulting colonies (of the relevant genotypes) were used to inoculate stock cultures (i.e., 48-h M2 colonies, radius ≈ 1 cm, stored at 4°C) and cultures for long-term stocks (i.e., explants from 48-h M2 colonies stocked in liquid RG medium at −75°C). For all experiments, to avoid alterations due to senescence or storage of the strains, cultures were inoculated with mycelial explants issued from fresh young M2 growing cultures at incubation distances <3 cm from the point of inoculation of the original ascospore yielding the corresponding strain. When required, media were supplemented with phleomycin (40 μg ml^{-1}), Geneticin (G418 sulfate, 100 μg ml^{-1}), nourseothricin (40 μg ml^{-1}), or hygromycin B (30 or 75 μg ml^{-1}, for gene tagging or deletions, respectively; see below). Current *P. anserina* methods and media can be found at http://podospora.i2bc.paris-saclay.fr.

Nucleic acid isolation, transformation, and plasmids. *P. anserina* genomic DNA isolation and the polyethylene glycol (PEG)-mediated protoplast transformation were performed as described in reference 88. The hygromycin resistance gene cassette used for gene deletions was derived from plasmid pBC-Hygro (89), and the *Streptomyces noursei nat1* gene from pAPI509 (a derivative from pAPI508 [87]). GFP-Hyg^R and mCherry-Hyg^R cassettes used for endogenous gene tagging were obtained from pUC-GFP and pUC-Cherry, respectively (90). pPable vector (91) was used for cloning *GFP*::*RTN1*. Plasmids GA0AA237CB11 (*P. anserina* genomic DNA library; Genoscope, France) and pSM334_Genticin were kindly provided by Robert Debuchy (Institute for Integrative Biology of the Cell, CNRS, France). Plasmid pCCG::N-GFP (92) was obtained from The Fungal Genetics Stock Center (Manhattan, KS, USA). Oligonucleotide primers used in this research are listed in Table S1 in the supplemental material.

Gene sequences. *RTN1* (*Pa_1_22550*), *YOP1* (*Pa_2_5730*), and *YOP2* (*Pa_4_3260*) gene sequences were obtained from the *P. anserina* genome sequence (https://genome.jgi.doe.gov/Podan2/Podan2.home.html). Their predicted protein sequences are available in the GenBank database under accession numbers CDP24655.1, CDP25565.1, and CDP28238.1, respectively. FUNGIpath v.4.0 (http://fungipath.i2bc.paris-saclay.fr [93]) was used to analyze for orthologous proteins in fungal genomes.

Gene deletions. Mutant strains deleted for *RTN1*, *YOP1*, and *YOP2* were generated by replacing their corresponding open reading frame (ORF) with a selectable marker by homologous recombination. *RTN1* and *YOP2* were replaced by the *hph* gene, while *YOP1* was replaced by the *nat1* gene. Gene replacement cassettes were generated by double-joint PCR (94) by flanking the selectable marker gene with ≈700 bp of the 5′ and 3′ flanking sequences of the ORF to be deleted. The 5′ fragment of these constructs was amplified with primers *gene-5F* and *gene-5R* (where *gene* indicates the corresponding deleted gene [Table S1]), and the 3′ fragment with primers *gene-3F* and *gene-3R*. The respective selectable marker gene was amplified with primers *gene-hph-F* and *gene-hph-R* (*yop1-nat-F* and *yop1-nat-R*, for YOP1). The generated gel-purified fusion PCR products were used to transform Δ*ku70* cells, and the obtained transformants were purified after sexual crosses to the wild type. Purified homokaryotic strains of both mating types (*mat*+ and *mat*−) and on the *KU70*$^+$ genetic background were recovered from the progeny of these crosses. Correct gene deletions were verified by PCR analyses.

Gene complementation analyses. For the gene complementation assays, protoplasts of the Δ*rtn1* strain were cotransformed with vector GA0AA237CB11, which harbors a copy of the *RTN1* gene, and pSM334_Genticin (in a 3:1 molar ratio). Eighteen Geneticin-resistant (Gen^R) transformants were randomly selected and analyzed for ascospore formation. Taking into account the recessive nature of the Δ*rtn1* sexual development phenotype, we inspected the restoration of ascospore formation in perithecia issued from heterozygous crosses of Δ*rtn1* to each Δ*rtn1*(Gen^R) transformant ($n \geq 100$ asci per strain). Four Δ*rtn1*(Gen^R) analyzed strains displayed a partial restoration of ascospore formation (i.e., producing between 8 and 13% of abnormal asci), and seven exhibited an ascospore formation restoration with levels of abnormal asci comparable to those of the wild type (0.8 to 3.7%). Three of these strains were further analyzed in triplicate experiments (Fig. S3).

Tagging of RTN1 and YOP2. We tagged RTN1 and YOP2 by fusing the coding sequence of GFP or mCherry to the 3′ end of their corresponding ORFs at their genomic loci. The tagging was attained by replacing the stop codon of *RTN1* or *YOP2* endogenous genes by a DNA cassette consisting of an in-frame fluorescent protein-encoding gene followed by a hygromycin resistance cassette (GFP-Hyg^R or mCherry-Hyg^R cassettes, respectively [90]) by homologous recombination. The tagging constructs were generated by fusion PCR and consisted of, for *RTN1*, (i) the last 720 bp (excluding the stop codon) of *RTN1* ORF 3′ end (amplified with primers *rtn1-F* and *lkt-rtn1*), fused in frame to (ii) the GFP-Hyg^R cassette from pUC-GFP (amplified with primers *rtn1-lkt* and *rtn1-hph-Ra*), and followed by (iii) 703 bp of DNA downstream *RTN1* stop codon (amplified with primers *hph-rtn1-Fa* and *rtn1-3R*). For *YOP2*, the construct

consisted of (i) the last 619 bp of *YOP2* ORF 3′ end (excluding the stop codon amplified with *yop2-F* and *lkt-yop2*), (ii) the mCherry-Hyg^R cassette from pUC-Cherry (amplified with *yop2-lkt* and *yop2-hph-Ra*), and (iii) 690 bp of DNA downstream *YOP2* stop codon (amplified with *hph-yop2-Fa* and *yop2-3R*). The fusion PCR-generated tagging cassettes were gel purified and used to transform protoplasts of a Δ*ku70* strain. Hyg^R transformants were randomly selected, and the Hyg^R marker was recovered in the *KU70*$^+$ genetic context after crosses to the wild type. *RTN1* and *YOP2* tagging was verified by PCR analyses and by sequencing.

Double-joint PCR was used to generate a *GFP*::*RTN1* gene to express RTN1 tagged with GFP at its N terminus. A DNA PCR fragment containing the *GFP* gene preceded by the *Neurospora crassa ccg-1* promoter was amplified from plasmid pCCG::N-GFP with primers *CCG1-F* and *rtn-GFP-R* and fused in frame to the coding sequence of the *RTN1* gene followed by 703 bp of its 3′ flanking sequence (amplified with primers *GFP-rtn-F* and *rtn1-3R*). The gel-purified fusion PCR product was cloned into plasmid pGEM-T Easy (Promega, Madison, WI), to be subcloned into the EcoRI site of plasmid pPable. The generated plasmid (pFS06) was verified by sequencing and used to transform Δ*rtn1* cells. A selected transformant was crossed to the wild-type strain, and the purified *GFP*::*RTN1* ectopic transgene was recovered from the progeny of this cross in homokaryotic strains of the Δ*rtn1* and *RTN1*$^+$ genetic backgrounds, respectively.

Vegetative growth and sexual reproduction analyses. Mycelial growth was determined by measuring the radius of mycelial colonies growing on M2 medium at 30°C every 24 h for 5 days. For each strain, three independent experiments, each with triplicates, were performed. The growth rate was defined as the slope of the corresponding growth curves. A two-way analysis of variance (ANOVA) using a Tukey *post hoc* analysis was performed to evaluate significant differences. Sexual development was analyzed as detailed recently (95); briefly, sexual crosses were performed by growing homokaryotic strains of opposite mating type on opposite sides of an M2 plate at 27°C in constant light for 3 days, after which they were cross-fertilized by spreading 2 ml of water over the colonies. Sexual cycle cells were obtained from perithecia issued from these crosses 4 days after fertilization.

Cytology. Sexual cycle cells were fixed in 7.4% paraformaldehyde and processed for fluorescence microscopy as described in reference 85. The ER was visualized using an ER-targeted GFP, which contained the ER targeting and retention signals of the putative *P. anserina* ER chaperone BiP (ER-GFP) (47). Nuclei and mitochondrial DNA were stained with DAPI (0.5 μg ml^{-1}), and the Spitzenkörper with the styryl dye FM4-64 [*N*-(3-triethylammoniumpropyl)-4-(6-(4-(diethylamino) phenyl) hexatrienyl) pyridinium dibromide, 7 μM] (Molecular Probes, Eugene, OR). To visualize the spindle apparatus, cells were labeled with mouse monoclonal (DM1A) anti-alpha-tubulin antibody (Abcam, Cambridge, United Kingdom; ab80779; dilution 1:1,000), using either fluorescein isothiocyanate (FITC)-conjugated (Jackson ImmunoResearch, West Grove, PA; 715-095-150; dilution 1:100) or Alexa Fluor 594-conjugated (Jackson ImmunoResearch; 715-585-150; dilution 1:100) donkey anti-mouse secondary antibodies. Live-cell microscopy was performed on growing leading hyphae from entire *P. anserina* colonies grown for 24 h on agarose beds of M2 medium containing 0.55% dextrin (90). To analyze the apical extension rate of individual hyphae, growing leading hyphae were imaged at 2-s intervals for 3 min using a 63× objective in a temperature chamber at 30°C. In the resulting time-lapse series, a segmented line tracing the trajectory of the hyphal tip across time was manually drawn, and a kymograph based on this line was plotted using the Reslice command of ImageJ. The slope of the kymograph line corresponding to the extending hyphal tip was used to determine the hypha apical extension rate. For each strain, 21 hyphae issued from 3 biological replicates (7 hyphae/replicate) were analyzed. The analysis of abundance of the apical ER subcompartments was done on confocal micrographs of the midplane of growing leading hypha expressing ER-GFP. For each strain, 40 hyphae issued from 4 biological replicates (10 hyphae/replicate) were analyzed. For each hypha, GFP images were thresholded using the Maximum Entropy algorithm and the area occupied by each apical ER patch was determined using the Particles analyzer in ImageJ. Statistical significance was determined by two-way ANOVA with Tukey's multiple-comparison test.

Microscopy. Epifluorescence microscopy was performed on a Nikon Eclipse E600 microscope using a cooled Neo Andor scientific complementary metal oxide semiconductor (sCMOS) camera. Confocal microscopy was done in a Zeiss LSM800 inverted laser scanning confocal microscope with a Plan-Apochromat 63×/1.4 oil immersion objective using 405-, 488-, and 561-nm laser lines. Bright-field images were acquired using the Electronically Switchable Illumination and Detection (ESID) module. For live-cell confocal microscopy, an equivalent Zeiss LSM800 system equipped with a temperature chamber (at 27°C) was used, and images from all channels were captured simultaneously. For three-dimensional (3D) imaging, z-section images were collected at 0.37- to 0.43-μm intervals through entire cell volumes. Images were processed using Zen 3.1 software (Carl Zeiss, Jena, Germany) or the FIJI package for ImageJ (96, 97).

SUPPLEMENTAL MATERIAL

Supplemental material is available online only.

FIG S1, PDF file, 1.2 MB.

FIG S2, PDF file, 0.1 MB.

FIG S3, PDF file, 2.4 MB.

TABLE S1, PDF file, 0.1 MB.

MOVIE S1, MOV file, 0.6 MB.

MOVIE S2, MOV file, 9.6 MB.

MOVIE S3, MOV file, 5.9 MB.

MOVIE S4, MOV file, 6.1 MB.
MOVIE S5, MOV file, 18 MB.
MOVIE S6, MOV file, 17.7 MB.

ACKNOWLEDGMENTS

We are grateful to Robert Debuchy (Institute for Integrative Biology of the Cell, CNRS, France) for kindly providing plasmids, to Ruth Rincón Heredia and Abraham Rosas Arellano (IFC Imaging Facility, UNAM) for assistance on microscopy, and to Jesús Aguirre and Wilhelm Hansberg (IFC, UNAM) for technical support. We thank Vladimir Orduña (Facultad de Psicología, UNAM) and members of the lab for fruitful discussions.

This work was supported by CONACYT, Mexico (grant CONACYT-DFG 277869), and by PAPIIT-DGAPA, UNAM, Mexico (grants IA201815 and AV200519]. A.D.J.L.-F. was supported by a scholarship from CONACYT. A.D.J.L.-F. and K.N.N.-G. were supported by scholarships from PAPIIT grant IA201815.

We declare no conflicts of interest in regard to this paper.

REFERENCES

1. Westrate LM, Lee JE, Prinz WA, Voeltz GK. 2015. Form follows function: the importance of endoplasmic reticulum shape. Annu Rev Biochem 84:791–811. https://doi.org/10.1146/annurev-biochem-072711-163501.
2. Schwarz DS, Blower MD. 2016. The endoplasmic reticulum: structure, function and response to cellular signaling. Cell Mol Life Sci 73:79–94. https://doi.org/10.1007/s00018-015-2052-6.
3. Carreras-Sureda A, Pihan P, Hetz C. 2018. Calcium signaling at the endoplasmic reticulum: fine-tuning stress responses. Cell Calcium 70:24–31. https://doi.org/10.1016/j.ceca.2017.08.004.
4. Hetz C, Zhang K, Kaufman RJ. 2020. Mechanisms, regulation and functions of the unfolded protein response. Nat Rev Mol Cell Biol 21:421–438. https://doi.org/10.1038/s41580-020-0250-z.
5. Karagöz GE, Aragón T, Acosta-Alvear D. 2019. Recent advances in signal integration mechanisms in the unfolded protein response. F1000Research 8:F1000 Faculty Rev-1840. https://doi.org/10.12688/f1000research.19848.1.
6. Rutkowski DT, Hegde RS. 2010. Regulation of basal cellular physiology by the homeostatic unfolded protein response. J Cell Biol 189:783–794. https://doi.org/10.1083/jcb.201003138.
7. Joshi AS, Zhang H, Prinz WA. 2017. Organelle biogenesis in the endoplasmic reticulum. Nat Cell Biol 19:876–882. https://doi.org/10.1038/ncb3579.
8. Phillips MJ, Voeltz GK. 2016. Structure and function of ER membrane contact sites with other organelles. Nat Rev Mol Cell Biol 17:69–82. https://doi.org/10.1038/nrm.2015.8.
9. Wu H, Carvalho P, Voeltz GK. 2018. Here, there, and everywhere: the importance of ER membrane contact sites. Science 361:eaan5835. https://doi.org/10.1126/science.aan5835.
10. De Magistris P, Antonin W. 2018. The dynamic nature of the nuclear envelope. Curr Biol 28:R487–R497. https://doi.org/10.1016/j.cub.2018.01.073.
11. LaJoie D, Ullman KS. 2017. Coordinated events of nuclear assembly. Curr Opin Cell Biol 46:39–45. https://doi.org/10.1016/j.ceb.2016.12.008.
12. Ungricht R, Kutay U. 2017. Mechanisms and functions of nuclear envelope remodelling. Nat Rev Mol Cell Biol 18:229–245. https://doi.org/10.1038/nrm.2016.153.
13. Shibata Y, Voss C, Rist JM, Hu J, Rapoport TA, Prinz WA, Voeltz GK. 2008. The reticulon and DP1/Yop1p proteins form immobile oligomers in the tubular endoplasmic reticulum. J Biol Chem 283:18892–18904. https://doi.org/10.1074/jbc.M800986200.
14. Voeltz GK, Prinz WA, Shibata Y, Rist JM, Rapoport TA. 2006. A class of membrane proteins shaping the tubular endoplasmic reticulum. Cell 124:573–586. https://doi.org/10.1016/j.cell.2005.11.047.
15. Shibata Y, Hu J, Kozlov MM, Rapoport TA. 2009. Mechanisms shaping the membranes of cellular organelles. Annu Rev Cell Dev Biol 25:329–354. https://doi.org/10.1146/annurev.cellbio.042308.113324.
16. Tolley N, Sparkes I, Craddock CP, Eastmond PJ, Runions J, Hawes C, Frigerio L. 2010. Transmembrane domain length is responsible for the ability of a plant reticulon to shape endoplasmic reticulum tubules in vivo. Plant J 64:411–418. https://doi.org/10.1111/j.1365-313X.2010.04337.x.
17. Zurek N, Sparks L, Voeltz G. 2011. Reticulon short hairpin transmembrane domains are used to shape ER tubules. Traffic 12:28–41. https://doi.org/10.1111/j.1600-0854.2010.01134.x.
18. Brady JP, Claridge JK, Smith PG, Schnell JR. 2015. A conserved amphipathic helix is required for membrane tubule formation by Yop1p. Proc Natl Acad Sci U S A 112:E639–E648. https://doi.org/10.1073/pnas.1415882112.
19. Breeze E, Dzimitrowicz N, Kriechbaumer V, Brooks R, Botchway SW, Brady JP, Hawes C, Dixon AM, Schnell JR, Fricker MD, Frigerio L. 2016. A C-terminal amphipathic helix is necessary for the in vivo tubule-shaping function of a plant reticulon. Proc Natl Acad Sci U S A 113:10902–10907. https://doi.org/10.1073/pnas.1605434113.
20. Hu J, Shibata Y, Voss C, Shemesh T, Li Z, Coughlin M, Kozlov MM, Rapoport TA, Prinz WA. 2008. Membrane proteins of the endoplasmic reticulum induce high-curvature tubules. Science 319:1247–1250. https://doi.org/10.1126/science.1153634.
21. Shibata Y, Shemesh T, Prinz WA, Palazzo AF, Kozlov MM, Rapoport TA. 2010. Mechanisms determining the morphology of the peripheral ER. Cell 143:774–788. https://doi.org/10.1016/j.cell.2010.11.007.
22. Wang N, Rapoport TA. 2019. Reconstituting the reticular ER network - mechanistic implications and open questions. J Cell Sci 132:jcs227611. https://doi.org/10.1242/jcs.227611.
23. Dawson TR, Lazarus MD, Hetzer MW, Wente SR. 2009. ER membrane-bending proteins are necessary for de novo nuclear pore formation. J Cell Biol 184:659–675. https://doi.org/10.1083/jcb.200806174.
24. Espadas J, Pendin D, Bocanegra R, Escalada A, Misticoni G, Trevisan T, Velasco Del Olmo A, Montagna A, Bova S, Ibarra B, Kuzmin PI, Bashkirov PV, Shnyrova AV, Frolov VA, Daga A. 2019. Dynamic constriction and fission of endoplasmic reticulum membranes by reticulon. Nat Commun 10:5327. https://doi.org/10.1038/s41467-019-13327-7.
25. Mukherjee RN, Levy DL. 2019. Reticulon 4a promotes exocytosis in mammalian cells. Mol Biol Cell 30:2349–2357. https://doi.org/10.1091/mbc.E19-03-0159.
26. Okamoto M, Kurokawa K, Matsuura-Tokita K, Saito C, Hirata R, Nakano A. 2012. High-curvature domains of the ER are important for the organization of ER exit sites in Saccharomyces cerevisiae. J Cell Sci 125:3412–3420. https://doi.org/10.1242/jcs.100065.
27. Wakana Y, Koyama S, Nakajima K, Hatsuzawa K, Nagahama M, Tani K, Hauri HP, Melancon P, Tagaya M. 2005. Reticulon 3 is involved in membrane trafficking between the endoplasmic reticulum and Golgi. Biochem Biophys Res Commun 334:1198–1205. https://doi.org/10.1016/j.bbrc.2005.07.012.
28. Casey AK, Dawson TR, Chen J, Friederichs JM, Jaspersen SL, Wente SR. 2012. Integrity and function of the Saccharomyces cerevisiae spindle pole body depends on connections between the membrane proteins Ndc1, Rtn1, and Yop1. Genetics 192:441–455. https://doi.org/10.1534/genetics.112.141465.
29. Pina FJ, Fleming T, Pogliano K, Niwa M. 2016. Reticulons regulate the ER inheritance block during ER stress. Dev Cell 37:279–288. https://doi.org/10.1016/j.devcel.2016.03.025.
30. Cho IT, Adelmant G, Lim Y, Marto JA, Cho G, Golden JA. 2017. Ascorbate peroxidase proximity labeling coupled with biochemical fractionation

identifies promoters of endoplasmic reticulum-mitochondrial contacts. J Biol Chem 292:16382–16392. https://doi.org/10.1074/jbc.M117.795286.
31. Reali V, Mehdawy B, Nardacci R, Filomeni G, Risuglia A, Rossin F, Antonioli M, Marsella C, Fimia GM, Piacentini M, Di Sano F. 2015. Reticulon protein-1C is a key component of MAMs. Biochim Biophys Acta 1853:733–745. https://doi.org/10.1016/j.bbamcr.2014.12.031.
32. David C, Koch J, Oeljeklaus S, Laernsack A, Melchior S, Wiese S, Schummer A, Erdmann R, Warscheid B, Brocard C. 2013. A combined approach of quantitative interaction proteomics and live-cell imaging reveals a regulatory role for endoplasmic reticulum (ER) reticulon homology proteins in peroxisome biogenesis. Mol Cell Proteomics 12:2408–2425. https://doi.org/10.1074/mcp.M112.017830.
33. Caldieri G, Barbieri E, Nappo G, Raimondi A, Bonora M, Conte A, Verhoef L, Confalonieri S, Malabarba MG, Bianchi F, Cuomo A, Bonaldi T, Martini E, Mazza D, Pinton P, Tacchetti C, Polo S, Di Fiore PP, Sigismund S. 2017. Reticulon 3-dependent ER-PM contact sites control EGFR nonclathrin endocytosis. Science 356:617–624. https://doi.org/10.1126/science.aah6152.
34. Grumati P, Morozzi G, Holper S, Mari M, Harwardt MI, Yan R, Muller S, Reggiori F, Heilemann M, Dikic I. 2017. Full length RTN3 regulates turnover of tubular endoplasmic reticulum via selective autophagy. Elife 6:e25555. https://doi.org/10.7554/eLife.25555.
35. Khaminets A, Heinrich T, Mari M, Grumati P, Huebner AK, Akutsu M, Liebmann L, Stolz A, Nietzsche S, Koch N, Mauthe M, Katona I, Qualmann B, Weis J, Reggiori F, Kurth I, Hubner CA, Dikic I. 2015. Regulation of endoplasmic reticulum turnover by selective autophagy. Nature 522:354–358. https://doi.org/10.1038/nature14498.
36. Zhang X, Ding X, Marshall RS, Paez-Valencia J, Lacey P, Vierstra RD, Otegui MS. 2020. Reticulon proteins modulate autophagy of the endoplasmic reticulum in maize endosperm. Elife 9:e51918. https://doi.org/10.7554/eLife.51918.
37. D'Eletto M, Oliverio S, Di Sano F. 2020. Reticulon homology domain-containing proteins and ER-phagy. Front Cell Dev Biol 8:90. https://doi.org/10.3389/fcell.2020.00090.
38. Rose MD. 1996. Nuclear fusion in the yeast Saccharomyces cerevisiae. Annu Rev Cell Dev Biol 12:663–695. https://doi.org/10.1146/annurev.cellbio.12.1.663.
39. Zickler D. 2006. Meiosis in mycelial fungi, p 415–438. *In* Kues U, Fisher R (ed), The mycota. I. Growth, differentiation and sexuality. Springer-Verlag, Berlin, Germany.
40. Zickler D, Espagne E. 2016. Sordaria, a model system to uncover links between meiotic pairing and recombination. Semin Cell Dev Biol 54:149–157. https://doi.org/10.1016/j.semcdb.2016.02.012.
41. Sato M, Kakui Y, Toya M. 2021. Tell the difference between mitosis and meiosis: interplay between chromosomes, cytoskeleton, and cell cycle regulation. Front Cell Dev Biol 9:660322. https://doi.org/10.3389/fcell.2021.660322.
42. Ng DT, Walter P. 1996. ER membrane protein complex required for nuclear fusion. J Cell Biol 132:499–509. https://doi.org/10.1083/jcb.132.4.499.
43. Nishikawa S, Endo T. 1997. The yeast JEM1p is a DnaJ-like protein of the endoplasmic reticulum membrane required for nuclear fusion. J Biol Chem 272:12889–12892. https://doi.org/10.1074/jbc.272.20.12889.
44. Normington K, Kohno K, Kozutsumi Y, Gething MJ, Sambrook J. 1989. S. cerevisiae encodes an essential protein homologous in sequence and function to mammalian BiP. Cell 57:1223–1236. https://doi.org/10.1016/0092-8674(89)90059-7.
45. Rose MD, Misra LM, Vogel JP. 1989. KAR2, a karyogamy gene, is the yeast homolog of the mammalian BiP/GRP78 gene. Cell 57:1211–1221. https://doi.org/10.1016/0092-8674(89)90058-5.
46. Vasnier C, de Muyt A, Zhang L, Tesse S, Kleckner NE, Zickler D, Espagne E. 2014. Absence of SUN-domain protein Slp1 blocks karyogamy and switches meiotic recombination and synapsis from homologs to sister chromatids. Proc Natl Acad Sci U S A 111:E4015–E4023. https://doi.org/10.1073/pnas.1415758111.
47. Lopez-Fuentes AJ, Meizoso-Huesca A, Peraza-Reyes L. 2020. An endoplasmic reticulum domain is associated with the polarized growing cells of Podospora anserina hyphae. Fungal Genet Biol 137:103338. https://doi.org/10.1016/j.fgb.2020.103338.
48. Markina-Inarrairaegui A, Pantazopoulou A, Espeso EA, Penalva MA. 2013. The Aspergillus nidulans peripheral ER: disorganization by ER stress and persistence during mitosis. PLoS One 8:e67154. https://doi.org/10.1371/journal.pone.0067154.
49. Maruyama J, Kikuchi S, Kitamoto K. 2006. Differential distribution of the endoplasmic reticulum network as visualized by the BipA-EGFP fusion protein in hyphal compartments across the septum of the filamentous fungus, Aspergillus oryzae. Fungal Genet Biol 43:642–654. https://doi.org/10.1016/j.fgb.2005.11.007.
50. Rico-Ramirez AM, Roberson RW, Riquelme M. 2018. Imaging the secretory compartments involved in the intracellular traffic of CHS-4, a class IV chitin synthase, in Neurospora crassa. Fungal Genet Biol 117:30–42. https://doi.org/10.1016/j.fgb.2018.03.006.
51. Wedlich-Soldner R, Schulz I, Straube A, Steinberg G. 2002. Dynein supports motility of endoplasmic reticulum in the fungus Ustilago maydis. Mol Biol Cell 13:965–977. https://doi.org/10.1091/mbc.01-10-0475.
52. Espagne E, Lespinet O, Malagnac F, Da Silva C, Jaillon O, Porcel BM, Couloux A, Aury JM, Segurens B, Poulain J, Anthouard V, Grossetete S, Khalili H, Coppin E, Dequard-Chablat M, Picard M, Contamine V, Arnaise S, Bourdais A, Berteaux-Lecellier V, Gautheret D, de Vries RP, Battaglia E, Coutinho PM, Danchin EG, Henrissat B, Khoury RE, Sainsard-Chanet A, Boivin A, Pinan-Lucarre B, Sellem CH, Debuchy R, Wincker P, Weissenbach J, Silar P. 2008. The genome sequence of the model ascomycete fungus Podospora anserina. Genome Biol 9:R77. https://doi.org/10.1186/gb-2008-9-5-r77.
53. Riquelme M, Aguirre J, Bartnicki-Garcia S, Braus GH, Feldbrugge M, Fleig U, Hansberg W, Herrera-Estrella A, Kamper J, Kuck U, Mourino-Perez RR, Takeshita N, Fischer R. 2018. Fungal morphogenesis, from the polarized growth of hyphae to complex reproduction and infection structures. Microbiol Mol Biol Rev 82:e00068-17. https://doi.org/10.1128/MMBR.00068-17.
54. Riquelme M, Sanchez-Leon E. 2014. The Spitzenkorper: a choreographer of fungal growth and morphogenesis. Curr Opin Microbiol 20:27–33. https://doi.org/10.1016/j.mib.2014.04.003.
55. Zickler D, Arnaise S, Coppin E, Debuchy R, Picard M. 1995. Altered mating-type identity in the fungus Podospora anserina leads to selfish nuclei, uniparental progeny, and haploid meiosis. Genetics 140:493–503. https://doi.org/10.1093/genetics/140.2.493.
56. Raju NB, Perkins DD. 1994. Diverse programs of ascus development in pseudohomothallic species of Neurospora, Gelasinospora, and Podospora. Dev Genet 15:104–118. https://doi.org/10.1002/dvg.1020150111.
57. Beckett A, Wilson IM. 1968. Ascus cytology of Podospora anserina. J Gen Microbiol 53:81–87. https://doi.org/10.1099/00221287-53-1-81.
58. Zickler D. 1970. Division spindle and centrosomal plaques during mitosis and meiosis in some Ascomycetes. Chromosoma 30:287–304. https://doi.org/10.1007/BF00321062.
59. Zickler D, Simonet JM. 1980. Identification of gene-controlled steps of ascospore development in Podospora anserina. Exp Mycol 4:191–206. https://doi.org/10.1016/0147-5975(80)90024-9.
60. Espagne E, Vasnier C, Storlazzi A, Kleckner NE, Silar P, Zickler D, Malagnac F. 2011. Sme4 coiled-coil protein mediates synaptonemal complex assembly, recombinosome relocalization, and spindle pole body morphogenesis. Proc Natl Acad Sci U S A 108:10614–10619. https://doi.org/10.1073/pnas.1107272108.
61. Simonet JM, Zickler D. 1972. Mutations affecting meiosis in Podospora anserina. I. Cytological studies. Chromosoma 37:327–351. https://doi.org/10.1007/BF00319874.
62. Chen S, Novick P, Ferro-Novick S. 2012. ER network formation requires a balance of the dynamin-like GTPase Sey1p and the Lunapark family member Lnp1p. Nat Cell Biol 14:707–716. https://doi.org/10.1038/ncb2523.
63. Pinar M, Penalva MA. 2021. The fungal RABOME: RAB GTPases acting in the endocytic and exocytic pathways of Aspergillus nidulans (with excursions to other filamentous fungi). Mol Microbiol 116:53–70. https://doi.org/10.1111/mmi.14716.
64. Verdín J, Bartnicki-Garcia S, Riquelme M. 2009. Functional stratification of the Spitzenkörper of Neurospora crassa. Mol Microbiol 74:1044–1053. https://doi.org/10.1111/j.1365-2958.2009.06917.x.
65. Verdín J, Sánchez-León E, Rico-Ramírez AM, Martínez-Núñez L, Fajardo-Somera RA, Riquelme M. 2019. Off the wall: the rhyme and reason of Neurospora crassa hyphal morphogenesis. Cell Surf 5:100020. https://doi.org/10.1016/j.tcsw.2019.100020.
66. Riquelme M, Bredeweg EL, Callejas-Negrete O, Roberson RW, Ludwig S, Beltrán-Aguilar A, Seiler S, Novick P, Freitag M. 2014. The Neurospora crassa exocyst complex tethers Spitzenkörper vesicles to the apical plasma membrane during polarized growth. Mol Biol Cell 25:1312–1326. https://doi.org/10.1091/mbc.E13-06-0299.
67. Liu Y, Vidensky S, Ruggiero AM, Maier S, Sitte HH, Rothstein JD. 2008. Reticulon RTN2B regulates trafficking and function of neuronal glutamate transporter EAAC1. J Biol Chem 283:6561–6571. https://doi.org/10.1074/jbc.M708096200.
68. Steiner P, Kulangara K, Sarria JC, Glauser L, Regazzi R, Hirling H. 2004. Reticulon 1-C/neuroendocrine-specific protein-C interacts with SNARE

proteins. J Neurochem 89:569–580. https://doi.org/10.1111/j.1471-4159.2004.02345.x.
69. De Craene JO, Coleman J, Estrada de Martin P, Pypaert M, Anderson S, Yates JR, III, Ferro-Novick S, Novick P. 2006. Rtn1p is involved in structuring the cortical endoplasmic reticulum. Mol Biol Cell 17:3009–3020. https://doi.org/10.1091/mbc.e06-01-0080.
70. Pinar M, Pantazopoulou A, Arst HN, Jr, Penalva MA. 2013. Acute inactivation of the Aspergillus nidulans Golgi membrane fusion machinery: correlation of apical extension arrest and tip swelling with cisternal disorganization. Mol Microbiol 89:228–248. https://doi.org/10.1111/mmi.12280.
71. Pinar M, Penalva MA. 2017. Aspergillus nidulans BapH is a RAB11 effector that connects membranes in the Spitzenkorper with basal autophagy. Mol Microbiol 106:452–468. https://doi.org/10.1111/mmi.13777.
72. D' Eletto M, Risuglia A, Oliverio S, Mehdawy B, Nardacci R, Bordi M, Di Sano F. 2019. Modulation of autophagy by RTN-1C: role in autophagosome biogenesis. Cell Death Dis 10:868. https://doi.org/10.1038/s41419-019-2099-7.
73. Vats S, Galli T. 2021. Introducing secretory reticulophagy/ER-phagy (SERP), a VAMP7-dependent pathway involved in neurite growth. Autophagy 17:1037–1039. https://doi.org/10.1080/15548627.2021.1883886.
74. Wojnacki J, Nola S, Bun P, Cholley B, Filippini F, Presse MT, Lipecka J, Lam SM, N'Guyen J, Simon A, Ouslimani A, Shui G, Fader CM, Colombo MI, Guerrera IC, Galli T. 2021. Role of VAMP7-dependent secretion of reticulon 3 in neurite growth. Cell Rep 35:109006. https://doi.org/10.1016/j.celrep.2021.109006.
75. Chong X, Wang C, Wang Y, Wang Y, Zhang L, Liang Y, Chen L, Zou S, Dong H. 2020. The dynamin-like GTPase FgSey1 plays a critical role in fungal development and virulence in Fusarium graminearum. Appl Environ Microbiol 86:e02720-19. https://doi.org/10.1128/AEM.02720-19.
76. Arai K, Sato M, Tanaka K, Yamamoto M. 2010. Nuclear compartmentalization is abolished during fission yeast meiosis. Curr Biol 20:1913–1918. https://doi.org/10.1016/j.cub.2010.09.004.
77. Asakawa H, Kojidani T, Mori C, Osakada H, Sato M, Ding DQ, Hiraoka Y, Haraguchi T. 2010. Virtual breakdown of the nuclear envelope in fission yeast meiosis. Curr Biol 20:1919–1925. https://doi.org/10.1016/j.cub.2010.09.070.
78. Asakawa H, Yang HJ, Hiraoka Y, Haraguchi T. 2016. Virtual nuclear envelope breakdown and its regulators in fission yeast meiosis. Front Cell Dev Biol 4:5. https://doi.org/10.3389/fcell.2016.00005.
79. De Souza CP, Osmani AH, Hashmi SB, Osmani SA. 2004. Partial nuclear pore complex disassembly during closed mitosis in Aspergillus nidulans. Curr Biol 14:1973–1984. https://doi.org/10.1016/j.cub.2004.10.050.
80. Osmani AH, Davies J, Liu HL, Nile A, Osmani SA. 2006. Systematic deletion and mitotic localization of the nuclear pore complex proteins of Aspergillus nidulans. Mol Biol Cell 17:4946–4961. https://doi.org/10.1091/mbc.e06-07-0657.
81. Casey AK, Chen S, Novick P, Ferro-Novick S, Wente SR. 2015. Nuclear pore complex integrity requires Lnp1, a regulator of cortical endoplasmic reticulum. Mol Biol Cell 26:2833–2844. https://doi.org/10.1091/mbc.E15-01-0053.
82. Jaspersen SL. 2021. Anatomy of the fungal microtubule organizing center, the spindle pole body. Curr Opin Struct Biol 66:22–31. https://doi.org/10.1016/j.sbi.2020.09.008.
83. Xiang X. 2018. Nuclear movement in fungi. Semin Cell Dev Biol 82:3–16. https://doi.org/10.1016/j.semcdb.2017.10.024.
84. Neiman AM. 2011. Sporulation in the budding yeast Saccharomyces cerevisiae. Genetics 189:737–765. https://doi.org/10.1534/genetics.111.127126.
85. Thompson-Coffe C, Zickler D. 1994. How the cytoskeleton recognizes and sorts nuclei of opposite mating type during the sexual cycle in filamentous ascomycetes. Dev Biol 165:257–271. https://doi.org/10.1006/dbio.1994.1251.
86. Raju NB, Newmeyer D. 1977. Giant ascospores and abnormal croziers in a mutant of Neurospora crassa. Exp Mycol 1:152–165. https://doi.org/10.1016/S0147-5975(77)80040-6.
87. El-Khoury R, Sellem CH, Coppin E, Boivin A, Maas MFPM, Debuchy R, Sainsard-Chanet A. 2008. Gene deletion and allelic replacement in the filamentous fungus Podospora anserina. Curr Genet 53:249–258. https://doi.org/10.1007/s00294-008-0180-3.
88. Coppin-Raynal E, Picard M, Arnaise S. 1989. Transformation by integration in Podospora anserina. III. Replacement of a chromosome segment by a two-step process. Mol Gen Genet 219:270–276. https://doi.org/10.1007/BF00261187.
89. Silar P. 1995. Two new easy to use vectors for transformations. Fungal Genet Rep 42:23. https://doi.org/10.4148/1941-4765.1353.
90. Suaste-Olmos F, Zirion-Martinez C, Takano-Rojas H, Peraza-Reyes L. 2018. Meiotic development initiation in the fungus Podospora anserina requires the peroxisome receptor export machinery. Biochim Biophys Acta Mol Cell Res 1865:572–586. https://doi.org/10.1016/j.bbamcr.2018.01.003.
91. Coppin E, Debuchy R. 2000. Co-expression of the mating-type genes involved in internuclear recognition is lethal in Podospora anserina. Genetics 155:657–669. https://doi.org/10.1093/genetics/155.2.657.
92. Honda S, Selker EU. 2009. Tools for fungal proteomics: multifunctional neurospora vectors for gene replacement, protein expression and protein purification. Genetics 182:11–23. https://doi.org/10.1534/genetics.108.098707.
93. Grossetete S, Labedan B, Lespinet O. 2010. FUNGIpath: a tool to assess fungal metabolic pathways predicted by orthology. BMC Genomics 11:81. https://doi.org/10.1186/1471-2164-11-81.
94. Kuwayama H, Obara S, Morio T, Katoh M, Urushihara H, Tanaka Y. 2002. PCR-mediated generation of a gene disruption construct without the use of DNA ligase and plasmid vectors. Nucleic Acids Res 30:E2. https://doi.org/10.1093/nar/30.2.e2.
95. Navarro-Espindola R, Takano-Rojas H, Suaste-Olmos F, Peraza-Reyes L. 2020. Distinct contributions of the peroxisome-mitochondria fission machinery during sexual development of the fungus Podospora anserina. Front Microbiol 11:640. https://doi.org/10.3389/fmicb.2020.00640.
96. Schindelin J, Arganda-Carreras I, Frise E, Kaynig V, Longair M, Pietzsch T, Preibisch S, Rueden C, Saalfeld S, Schmid B, Tinevez JY, White DJ, Hartenstein V, Eliceiri K, Tomancak P, Cardona A. 2012. Fiji: an open-source platform for biological-image analysis. Nat Methods 9:676–682. https://doi.org/10.1038/nmeth.2019.
97. Schneider CA, Rasband WS, Eliceiri KW. 2012. NIH Image to ImageJ: 25 years of image analysis. Nat Methods 9:671–675. https://doi.org/10.1038/nmeth.2089.